# RIS-aided Cell-Free Massive MIMO Systems with Channel Aging

Enyu Shi, *Graduate Student Member, IEEE*, Jiayi Zhang, *Senior Member, IEEE*, Jiakang Zheng, *Graduate Student Member, IEEE*, Bo Ai, *Fellow, IEEE*, and Derrick Wing Kwan Ng, *Fellow, IEEE*

***Abstract*—Cell-free (CF) massive multiple-input multiple-output (MIMO) and reconfigurable intelligent surface (RIS) are two disruptive technologies for enabling the sixth-generation network. In this paper, we investigate the effect of channel aging on the RIS-aided CF massive MIMO systems over spatially correlated channels. We consider a minimum mean square error channel estimator that facilitates the derivation of closed-form spectral efficiency expressions. For the uplink, we compare the large-scale fading decoding method with the centralized decoding method. For the downlink, we adopt the maximum ratio precoding and propose a practical fractional power control method to improve the performance. Based on the analytical framework, we unveil the interplay between channel aging, spatial correlation, and signal processing methods. Our results demonstrate that the RIS-aided CF massive MIMO system outperforms the conventional CF counterpart system in both static and mobile scenarios. Moreover, when the link is weak, the introduction of RIS can lead to even more substantial performance enhancement. Also, RIS can be deployed to compensate for system performance degradation caused by channel aging and potentially lead to energy savings, while still achieving excellent performance. Intriguingly, due to the mutual coupling of RIS element and AP antenna correlations, RIS can effectively mitigate the negative effects caused by spatial correlation among AP antennas. Furthermore, we provide a practical rule-of-thumb guideline for designing resource block length, accounting for the impacts caused by channel aging.**

***Index Terms*—Reconfigurable intelligent surface, cell-free massive MIMO, channel aging, spatial correlation, spectral efficiency.**

## I. Introduction

To satisfy the demand for high mobility, low-latency, high spectral efficiency (SE), low-power consumption wireless communications imposed by the upcoming sixth-generation (6G) networks, various promising technologies have been introduced in the last few decades [1], including massive multiple-input multiple-output (MIMO), millimeter-wave communications, network densification, etc. Among them, cell-free (CF) massive MIMO wireless network structures, which consist of a central processing unit (CPU) connected to a large number of access points (APs) for coherently serving numerous user equipments (UEs) with the same time-frequency resource [2], stands out as the evolution of the conventional massive MIMO technology. Compared with traditional cellular systems, the characteristic of CF massive MIMO offers a sharp tool to circumvent the problem of strong inter-cell interference, which is the main inherent performance limitation in densely deployed cellular networks [3].

Recently, various important aspects and fundamentals of CF massive MIMO have been explored to unlock its potential. For example, [2] studied the CF massive MIMO system performance which adopts the effective maximum ratio (MR) processing based on the distributed implementation, while [3] introduced the fully centralized signal processing in the traditional CF mMIMO system with the minimum mean square error (MMSE) combining scheme achieving high spectral efficiency (SE). In addition, in contrast to the simple centralized decoding (SCD), i.e., the same weight coefficient is adopted for decoding across different APs, the two-layer decoding method for CF massive MIMO is believed to serve as an effective signal decoding scheme exploiting the MR/MMSE combining methods in the first layer decoder at the APs and the large-scale fading decoding (LSFD) method in the second layer decoder at the CPU [4], [5]. Unfortunately, CF massive MIMO still cannot guarantee an ideal quality of service (QoS) for multiple users, under some harsh propagation conditions such as in the practical cases of severe attenuation due to the presence of large obstacles or poor scattering environment [6].

Reconfigurable intelligent surface (RIS) is considered as a promising technology which can adaptively alter the propagation environment without applying expensive power amplifiers and complex digital signal processing methods [7]. Specifically, RIS can adapt the phase of the reflected signals with massive passive reflective elements to realize effective beamforming [8]. Moreover, we can flexibly deploy the RIS to assist the users with unfavorable channel conditions to significantly improve their QoS in a cost-effective manner [9]. Notably, due to its unique structural characteristics, RIS is different from the traditional uniform linear array (ULA) from various aspects. For example, it has been shown in [10] that the spatial correlation among RIS elements can be modeled as a sinc function. Based on this, in [11], [12], the authors explored the impact of the elements' spatial correlation on RIS-assisted communications and indicated that the correlation can cause significant system performance degradation if it is ignored. Meanwhile, RIS spatial correlations are generally coupled

This work was supported in part by the Fundamental Research Funds for the Central Universities under Grants 2023YJS015 and 2022JBQY004, in part by National Natural Science Foundation of China under Grants 62221001, in part by Natural Science Foundation of Jiangsu Province, Major Project under Grant BK20212002, and in part by ZTE Industry-University-Institute Cooperation Funds under Grant No. HC-CN-20221202003. (*Corresponding author: Jiayi Zhang*).

E. Shi, J. Zhang, J. Zheng, and B. Ai are with the School of Electronics and Information Engineering and Frontiers Science Center for Smart High-speed Railway System, Beijing Jiaotong University, Beijing 100044, P. R. China. (e-mail: enyushi,jiayizhang,jiakangzheng@bjtu.edu.cn).

D. W. K. Ng is with the School of Electrical Engineering and Telecommunications, University of New South Wales, NSW 2052, Australia. (e-mail: w.k.ng@unsw.edu.au).

with many factors, e.g., other correlations in the antennas of wireless transceivers, and their joint impacts on the system performance are still far from being understood that calls for a thorough investigation.

Inspired by their potentials, various works have focused on novel designs for jointly exploiting the advantages of the CF massive MIMO and the RIS to further improve system communication performance, e.g., [13]–[17]. Specifically, the authors in [13] proposed a joint precoding framework and designed an alternating optimization approach to further improve the sum-rate of all the UEs in RIS-aided CF massive MIMO systems. Besides, [6] proposed an effective aggregated channel estimation approach to acquire the channel coefficients and investigated the RIS-aided CF massive MIMO system with the MR combining over spatially-correlated channels. In addition, the authors in [18] designed the joint precoding of RIS-aided CF massive MIMO systems, utilizing a distributed machine learning-based approach to enhance system performance. Furthermore, aiming to improve the system capacity and energy efficiency, a wireless energy transfer framework for RIS-aided CF massive MIMO systems was introduced in [14]. It was shown that effective fractional power control (FPC) can improve the performance of RIS-aided CF systems in the downlink. In [19], the authors introduced a joint RIS beamforming and power control method in both single-cell and multi-cell networks to maximize SE. Besides, in [20], the non-convex problem of power allocation for the downlink global energy efficiency maximization was addressed at millimeter wave frequencies in CF mMIMO systems. However, the aforementioned works only consider the static scenarios of UEs where the channel realization is approximately constant in each coherence time resource block. In practice, due to the mobility of UEs, practical channels are varying continuously such that the channel coefficients are different across time but still correlated in a transmission block leading to the so-called channel aging [21]. In fact, some previous works have investigated the impact of channel aging on traditional MIMO systems. For example, the authors in [22] exploited the temporal channel correlation in channel aging for predicting the future channel conditions in massive MIMO systems by adopting the technique of machine learning. Specifically, it requires a substantial amount of training data in the initial stages to ensure the accuracy of the results. Furthermore, the authors in [23], [24] analyzed the performance degradation caused by channel aging on the downlink achievable sum SE in massive MIMO systems by adopting regularized zero-forcing (RZF) signal precoding at the APs and applying the deterministic equivalent (DE) analysis. Also, the joint consideration for the spatial correlations of RIS elements and AP antennas was analyzed which are crucial in determining the system performance. In addition, the authors in [25] proposed a channel aging-aware precoding (CAP) algorithm for maximizing the sum rate of RIS-aided multi-user communications. These results demonstrate that the CAP can improve system performance at the cost of high computational complexity. Besides, various works have studied the impact of channel aging on CF massive MIMO systems. For instance, in [26], the authors presented a new model for capturing the characteristic of the temporal evolution of the channel and derived the DE of the SINR. Also, in [27], the authors derived the closed-form expressions of SE with LSFD and analyzed the impact of channel aging in CF massive MIMO systems. These results highlight the advantages of CF massive MIMO systems in terms of channel aging compared to conventional cellular systems. However, the practical two-layer signal processing architecture of RIS-aided CF massive MIMO systems was not studied in [26], [27] and the spatial correlations and mobility effects on the distributed decoding implementation remain unknown. Therefore, the performance boundaries and practical architecture design of RIS-aided CF massive MIMO systems for practical implementation in mobility scenarios remain unknown and should be thoroughly analyzed.

Motivated by the aforementioned discussions, we investigate the impact of channel aging on the uplink and downlink performance of RIS-aided CF massive MIMO systems over spatially correlated channels. More specifically, we propose the MMSE channel estimation approach to estimate the channels between the UEs and the APs. For the uplink, utilizing the obtained channel estimates, we consider MR combining at the APs and the SCD or LSFD cooperations at the CPU. We compare the RIS-aided CF massive MIMO system performance with the CF system in the presence of channel aging. As for the downlink, exploiting the estimated channel state information, we utilize the MR precoding at the APs and analyze the corresponding system performance. Then, a practical fractional power control (FPC) scheme is proposed to further improve the considered downlink system performance. Also, we design a channel aging aware scheme in the resource block to improve the sum SE. The specific contributions of this work are listed as follows:

- We first propose a channel aging analysis framework of the RIS-aided CF massive MIMO system and derive the closed-form expressions for the uplink and downlink SE. In particular, we adopt a two-stage signal processing method to fully utilize the advantages of the CF network architecture. Our results show that in both mobile and static scenarios, the RIS-aided CF massive MIMO system outperforms the CF system in both uplink and downlink. Specifically, when the channel of the direct link is in deep fade, the above performance improvement is more significant.
- We analyze the impact of different system parameters and channel aging on the system performance, such as the number of RIS elements, Doppler shift, spatial correlation, transmit power, and the length of the resource block. We find that it is beneficial to increase the number of RIS elements with SCD and LSFD, even with a non-adaptive RIS phase shift, but with diminishing returns when the number of RIS elements is sufficiently large. Also, with the deployment of multiple RISs, the system only requires a lower power consumption than the CF system to achieve the corresponding SE upper bound. Moreover, the existence of spatial correlations of RIS elements and AP antennas reduces the SE. Also, compared with conventional CF massive MIMO systems, our

analyses reveal that the performance of the RIS-aided CF massive MIMO system is more sensitive to the amount of available pilot resources in the existence of channel aging. In particular, RIS can effectively compensate for the performance degradation caused by channel aging, especially if the latter is severe.

- We design a channel-aging-aware FPC method to resist channel aging for practical implementation. Our results show that the proposed FPC scheme can further improve the SE of the UEs with poor channel conditions and serious channel aging. Compared with CF massive MIMO, RIS-aided CF massive MIMO can effectively compensate the degradation of system performance caused by channel aging such that the resource block length only introduces a relatively insignificant impact on the sum SE. Besides, by introducing a training phase in front of downlink resource blocks, channel aging can be effectively combated. Also, different from the fixed resource block length scheme which has unstable performance considering channel aging, by carefully adopting the channel aging aware design scheme in the block, the issue of channel aging in the RIS-aided CF system can be alleviated to a large extent.

The rest of this paper is organized as follows. In Section II, we present the adopted RIS-aided CF massive MIMO system model incorporating the effects of spatial correlation, channel aging, and pilot contamination. Next, in Section III, the achievable system SE in the uplink is presented by considering the impact of channel aging for both the SCD and LSFD cooperations. Then, we present the achievable downlink SE and design a practical FPC to further explore the potential of the system performance with channel aging in Section IV. Numerical results and performance analysis are provided in Section V. Finally, Section VI concludes the paper.

**Notation:** The matrices and column vectors are denoted by boldface uppercase letters $\mathbf{X}$ and boldface lowercase letters $\mathbf{x}$, respectively. The superscripts $\mathbf{x}^{\mathrm{H}}$, $\mathbf{x}^{\mathrm{T}}$, and $x^*$ are used to represent conjugate transpose, transpose, and conjugate, respectively. $(\cdot)^{-1}$ represents the matrix inverse. $\mathbb{C}^{N\times M}$ represents complex matrices with space $N \times M$. $\|\cdot\|$ and $\lfloor\cdot\rfloor$ represent the Euclidean norm and the truncated argument, respectively. $\mathrm{mod}\,(\cdot,\cdot)$ and $\mathrm{tr}\,(\cdot)$ represent the modulus and the trace operations, respectively. $\mathrm{Cov}\,\{\cdot\}$ and $\mathbb{E}\,\{\cdot\}$ are the covariance and the expectation operators. The block-diagonal matrix with variables $x_1,\ldots,x_m$ on the diagonal is denoted by $\mathrm{diag}\,(x_1,\ldots,x_n)$. The definition is denoted by $\triangleq$ and $\mathrm{sinc}\,(x)=\sin(\pi x)/(\pi x)$ represents the sinc function. $\{x\colon y=z\}$ denotes that $x$ obeys the constraint $y=z$. $x\sim\mathcal{CN}\left(0,\sigma^2\right)$ denotes the circularly symmetric complex Gaussian random variable $x$ with variance $\sigma^2$. Finally, $[\mathbf{R}]_{mn}$ represents the element in row $m$ and column $n$ of matrix $\mathbf{R}$.

## II. System Model

As depicted in Fig. 1, we consider a RIS-aided CF massive MIMO system with $L$ APs, $K$ mobile UEs, $T$ RISs, and a CPU. We assume that each AP is equipped with $N$ antennas and each UE has a single antenna. The RIS consists of $M$ reflective elements that can introduce different phase shifts

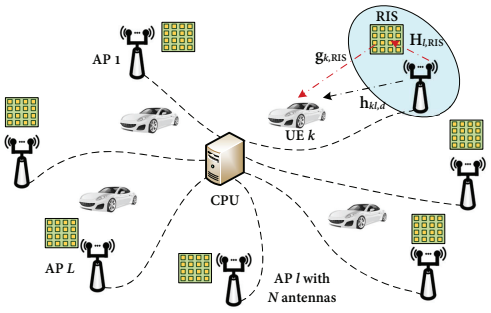


Fig. 1: An RIS-aided CF massive MIMO system with multiple mobile UEs, a CPU, and RISs.

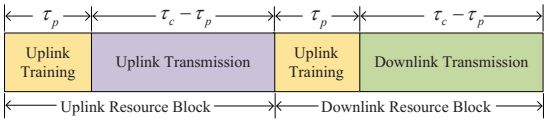


Fig. 2: Uplink and downlink resource block of the considered system.

to the impinging signals. We assume that the UEs travel at different speeds causing channel variations across time. Due to the mobility of UEs, deploying RISs in close proximity to all UEs is not possible. As a result, we assume that each deployed RIS is close to only one AP such that $T = L$. By doing so, it is guaranteed that the beam reflected from the RIS can be effectively focused on the desired AP, while keeping the interference caused by other RISs sufficiently weak to be negligible [11]. Also, the APs and the RISs are connected to the CPU via ideal fronthaul links for conveying the received signal at the APs [3]. We consider all the $K$ UEs are simultaneously served by all the $L$ APs on the same time-frequency resource. Besides, we assume the time-division duplex (TDD) protocol, as shown in Fig. 2, where there are two different types of blocks: one for the uplink data and another for the downlink data.[1] In both the uplink and downlink blocks, we assume that $\tau_p$ time instants are exploited for the uplink pilot training, while the remaining $\tau_c-\tau_p$ time instants are utilized for both the uplink and downlink data transmission.

### A. Channel Model

As shown in Fig. 1, the channels are divided into two types: the direct links from the UEs to the APs and the cascaded links through the RIS. Let $\mathbf{h}_{kl,d}\in\mathbb{C}^N$ be the direct link channel between AP $l$, $l\in\{1,\ldots,L\}$, and UE $k$, $k\in\{1,\ldots,K\}$. $\mathbf{H}_{l,\mathrm{RIS}}\in\mathbb{C}^{N\times M}$ denotes the channel matrix from AP $l$ to the RIS and $\mathbf{g}_{k,\mathrm{RIS}}\in\mathbb{C}^M$ denotes the channel from the RIS to UE $k$. Meanwhile, a practical model is considered to capture the spatial correlation among the RIS reflecting elements [10]. Besides, we consider an urban environment where multiple scatters exist without dominated line-of-sight (LoS) paths to

[1]The estimated channel information becomes outdated over time due to channel aging such that the system performance is worsen over time. Hence, to ensure the fairness of uplink and downlink UEs performance, we assume that the uplink and downlink data is transmitted in different resource blocks to ensure that both the uplink and downlink can utilize the most accurate channel estimates in each resource block [28].

UEs. Thus, we consider that $\mathbf{h}_{kl,d}$ and $\mathbf{g}_{k,\mathrm{RIS}}$ at the $n$th time instant follows correlated Rayleigh fading channel models that are given by

$$\mathbf{h}_{kl,d}[n] \sim \mathcal{CN}(\mathbf{0}, \mathbf{R}_{kl,d}), \quad n = 0, 1, \ldots, \tau_c, \tag{1}$$

$$\mathbf{g}_{k,\mathrm{RIS}}[n] \sim \mathcal{CN}(\mathbf{0}, \mathbf{R}_{k,\mathrm{RIS}}), \quad n = 0, 1, \ldots, \tau_c, \tag{2}$$

respectively, where $\mathbf{R}_{kl,d} \in \mathbb{C}^{N\times N}$ and $\mathbf{R}_{k,\mathrm{RIS}} = \beta_{k,\mathrm{RIS}} A \mathbf{R}_r \in \mathbb{C}^{M\times M}$ are the spatially correlated matrices of AP $l$'s antennas and the RIS elements, respectively. $\beta_{kl,d} \triangleq \mathrm{tr}(\mathbf{R}_{kl,d})/N$ and $\beta_{k,\mathrm{RIS}} \triangleq \mathrm{tr}(\mathbf{R}_{k,\mathrm{RIS}})/AM$ are the large-scale fading coefficients of the AP $l$-UE $k$ and the RIS-UE $k$ links, respectively. The spatial correlated matrices $\mathbf{R}_{kl,d}\,\forall l, k$, and $\mathbf{R}_{k,\mathrm{RIS}}\,\forall k$, are determined by the location of the devices in the system and the inherent hardware properties of the RIS, and therefore existing estimation methods can be adopted to obtain them [5]. Variable $A = d_H d_V$ represents the area of each RIS element, where $d_H$ and $d_V$ represent the horizontal width and the vertical height of each element, respectively. $\mathbf{R}_r \in \mathbb{C}^{M\times M}$ is the spatial correlation matrix of the RIS elements and its $(n', m')$-th element is expressed as $[\mathbf{R}]_{n'm'} = \mathrm{sinc}(2\|\mathbf{u}_{n'} - \mathbf{u}_{m'}\|/\lambda)$, where the position vector $\mathbf{u}_x$ is expressed as $\mathbf{u}_x = [0, \mathrm{mod}(x-1, N_H) d_H, \lfloor (x-1)/N_H \rfloor d_V]^{\mathrm{T}}$, $x \in \{n', m'\}$ and $\lambda$ represents the carrier wavelength of the carrier frequency [10]. $N_V$ and $N_H$ are the number of elements in each column and row at the RIS, respectively, such that $N = N_V \times N_H$.

Different from the mobile UEs, the locations of the APs and the RIS are generally fixed, and in practice, the RIS is deployed at a position having an LoS to the APs to enhance the communication for the UEs [24], [25]. Without loss of generality, we assume that the direct link and the cascaded link through RIS are independent and uncorrelated.[2] As such, the low-rank LoS channel $\mathbf{H}_{l,\mathrm{RIS}}$ can be described as [24]

$$[\mathbf{H}_{l,\mathrm{RIS}}]_{nm} = \sqrt{\beta_{l,\mathrm{RIS}}} \exp\Big( j\frac{2\pi}{\lambda}(n-1) d_{\mathrm{AP}} \sin\theta_{l,\mathrm{RIS},m} \times \sin\phi_{l,\mathrm{RIS},m} + (m-1) d_{\mathrm{RIS}} \sin\theta_{l,n} \sin\phi_{l,n} \Big), \tag{3}$$

where $\beta_{l,\mathrm{RIS}}$ is the path loss between AP $l$ and the RIS, $d_{\mathrm{RIS}}$ and $d_{\mathrm{AP}}$ are the inter-element separation of the RIS and the inter-antenna separation of the AP, respectively. Besides, $\phi_{l,\mathrm{RIS},m}$ and $\theta_{l,\mathrm{RIS},m}$ are the azimuth and elevation LoS angles of departure (AoD) at AP $l$ with respect to RIS element $m$, while $\phi_{l,n}$ and $\theta_{l,n}$ denote the azimuth and elevation LoS angles of arrival (AoA) at the RIS.

Let $\mathbf{\Theta} = \mathrm{diag}\left(e^{j\theta_1}, e^{j\theta_2}, \cdots, e^{j\theta_M}\right)$ represent the phase shift matrix of the $M$ elements, where $\theta_m \in [-\pi, \pi], \forall m \in \{1, \ldots, M\}$, is the phase shift for the $m$-th element of the RIS. Thus, the total aggregated channel between AP $l$ and UE $k$ can be formulated as

$$\mathbf{o}_{kl}[n] = \mathbf{h}_{kl,d}[n] + \mathbf{H}_{l,\mathrm{RIS}} \mathbf{\Theta} \mathbf{g}_{k,\mathrm{RIS}}[n], \forall n, \tag{4}$$

which consists of the cascaded link reflected by the RIS and the direct link from AP $l$ to UE $k$. Note that the adaptive phase shift design for RIS usually relies on the availability of instantaneous CSI. By contrast, we investigate the system performance on a long-time scale in which the non-adaptive phase shifts design of RIS does not have a significant impact on the system performance. For simplicity, but without loss of generality, we assume that the phase shifts of RIS are all set equal to $\frac{1}{4}\pi$ as the one adopted in [6]. Now, we derive the second-order statistic of $\mathbf{o}_{kl}[n]$ which will facilitate the performance analysis in the following sections. The covariance matrix of the channel $\mathbf{o}_{kl}[n]$ in (4) is derived as

$$\begin{aligned}
&\mathbb{E}\left\{\mathbf{o}_{kl}[n]\, \mathbf{o}_{kl}^{\mathrm{H}}[n]\right\} \\
&= \mathbb{E}\left\{\mathbf{h}_{kl,d}[n]\, \mathbf{h}_{kl,d}^{\mathrm{H}}[n]\right\} \\
&+ \mathbb{E}\left\{\mathbf{H}_{l,\mathrm{RIS}} \mathbf{\Theta} \mathbf{g}_{k,\mathrm{RIS}}[n]\, \mathbf{g}_{k,\mathrm{RIS}}^{\mathrm{H}}[n]\, \mathbf{\Theta}^{\mathrm{H}} \mathbf{H}_{l,\mathrm{RIS}}^{\mathrm{H}}\right\} \\
&= \mathbf{R}_{kl,d} + \mathbf{H}_{l,\mathrm{RIS}} \mathbf{\Theta} \mathbf{R}_{k,\mathrm{RIS}} \mathbf{\Theta}^{\mathrm{H}} \mathbf{H}_{l,\mathrm{RIS}}^{\mathrm{H}}.
\end{aligned} \tag{5}$$

In the following, we denote the aggregated channel is distributed as $\mathbf{o}_{kl}[n] \sim \mathcal{CN}(\mathbf{0}, \mathbf{R}_{kl})$ where $\mathbf{R}_{kl} \triangleq \mathbf{R}_{kl,d} + \mathbf{H}_{l,\mathrm{RIS}} \mathbf{\Theta} \mathbf{R}_{k,\mathrm{RIS}} \mathbf{\Theta}^{\mathrm{H}} \mathbf{H}_{l,\mathrm{RIS}}^{\mathrm{H}}$.

**Remark 1.** *Note that if the spatially correlated matrix of RIS elements $\mathbf{R}_r = \mathbf{I}_M$ is considered, the overall covariance becomes $\mathbf{R}_{kl} = \mathbf{R}_{kl,d} + \beta_{k,\mathrm{RIS}} A \mathbf{H}_{l,\mathrm{RIS}} \mathbf{H}_{l,\mathrm{RIS}}^{\mathrm{H}}$. In this case, $\mathbf{R}_{kl}$ is independent of the non-adaptive reflecting beamforming matrix at the RIS such that the phase shifts of the RIS do not have an impact on the long timescale system performance.*

### B. Channel Aging

In practice, the existence of channel aging leads to outdated channel estimates, which has been shown to affect system performance significantly [25]. Mathematically, the aggregated channel $\mathbf{o}_{kl}[n]$ at time instant $n$ can be modeled as a function of its initial state $\mathbf{o}_{kl}[0]$ and an innovation component [27], which can be modeled as

$$\mathbf{o}_{kl}[n] = \rho_k[n]\, \mathbf{o}_{kl}[0] + \bar{\rho}_k[n]\, \mathbf{e}_{kl}[n], \forall k, l, n, \tag{6}$$

where $\rho_k[n]$ denotes the temporal correlation coefficient between the channel realizations of UE $k$ at time 0 and $n$, while $\bar{\rho}_k[n] = \sqrt{1 - \rho_k^2[n]}$. Besides, $\mathbf{e}_{kl}[n] \sim \mathcal{CN}(\mathbf{0}, \mathbf{R}_{kl})$ is the channel independent component at time instant $n$. Without loss of generality, we consider $\rho_k[n] = J_0(2\pi f_{D,k} T_s n)$ with $J_0(\cdot)$ being the zeroth-order Bessel function of the first kind [29, Eq. (9.1.18)], where $f_{D,k} = (v_k f_c)/c$ is the Doppler shift experienced by UE $k$.[3] Subsequently, $v_k$, $c$, and $f_c$ denote the velocity of UE $k$, the speed of light, and the carrier frequency, respectively. $T_s$ represents the channel sampling duration. It is not difficult to find that a higher speed of a UE or a longer delay generally results in the decreases of $\rho_k[n]$, although not always monotonically.

[2]We focus on the impact of spatial correlation due to angle and antenna spacing. For this reason, we do not consider the correlation between the direct link and the cascaded link incoming signals at the observation by the APs although it might exist [11], [17].

[3]The adopted Jakes model is often employed to describe channel aging, e.g., [21], which assumes a two-dimensional isotropic scatter with a vertical monopole antenna equipped at the receiver. Due to the isotropy assumption, the variety in velocity caused by different angles resulting from the positions of the AP and RIS does not affect the modeling given by the $J_0(\cdot)$ function. Therefore, we assume that the velocities of UEs with respect to the AP and RIS are identical such that we can apply one Jake model to capture the channel aging characteristic of both the AP-UE and RIS-UE channels.

### C. Uplink Pilot Training and Channel Estimation

In practical RIS-aided CF massive MIMO systems, it is difficult to capture perfect channel state information (CSI) and the APs need to estimate the channel via exploiting pilot training sequences [17]. Hence, we impose an assumption that $\tau_p$ mutually orthogonal time-multiplexed pilot sequences are employed. This implies that pilot sequence $t$ represents the transmission of a pilot signal only at time instant $t$ within the resource block. This pilot design is crucial for maintaining orthogonality between the pilots, particularly in the presence of channel aging [27], [30]. $t_k \in \{1,\ldots,\tau_p\}$ denotes the index of the time instant adopted by UE $k$ and $\mathcal{P}_k \in \{i : t_i = t_k\} \subset \{1,\ldots,K\}$ denotes the UEs that adopt the same time instant for pilot transmission with UE $k$. The received signal at AP $l$ in time instant $t_k$ is denoted as

$$\mathbf{z}_l\left[t_k\right] = \sum_{i\in\mathcal{P}_k} \sqrt{p_i}\mathbf{o}_{il}\left[t_i\right] + \mathbf{w}_l\left[t_k\right], \tag{7}$$

where $\mathbf{w}_l\left[t_k\right] \sim \mathcal{CN}\left(\mathbf{0}, \sigma^2\mathbf{I}_N\right)$ denotes the noise at AP $l$ and $\sigma^2$ is the noise power per antenna. $p_i \geq 0$ denotes the pilot transmission power by UE $i$. We can exploit the received signal to estimate the channels at any time instant in a block. In order to ensure the accuracy of the estimated channels, we estimate the channels at $\varepsilon = \tau_p + 1$ time instant. Subsequently, these estimated channels are adopted as the initial states to obtain the estimation of the aggregated channels for the later time instants. Hence, the $t_i$th time instant channel between UE $i$ and AP $l$ can be denoted by the channel at instant $\varepsilon$ as

$$\mathbf{o}_{il}\left[t_i\right] = \rho_i\left[\varepsilon - t_i\right]\mathbf{o}_{il}\left[\varepsilon\right] + \bar{\rho}_i\left[\varepsilon - t_i\right]\mathbf{f}_{il}\left[t_i\right], \tag{8}$$

where $\mathbf{f}_{il}\left[t_i\right] \sim \mathcal{CN}\left(\mathbf{0}, \mathbf{R}_{kl}\right)$ is the independent innovation component which relates $\mathbf{o}_{il}\left[\varepsilon\right]$ and $\mathbf{o}_{il}\left[t_i\right]$. By utilizing (8), we can rewrite (7) as

$$\begin{aligned}\mathbf{z}_l\left[t_k\right] =& \sum_{i\in\mathcal{P}_k}\sqrt{p_i}\rho_i[\varepsilon - t_i]\,\mathbf{o}_{il}\left[\varepsilon\right] + \sum_{i\in\mathcal{P}_k}\sqrt{p_i}\bar{\rho}_i[\varepsilon - t_i]\mathbf{f}_{il}\left[t_i\right] + \mathbf{w}_l[t_k] \\ =& \underbrace{\sqrt{p_k}\rho_k\left[\varepsilon - t_k\right]\mathbf{o}_{kl}\left[\varepsilon\right]}_{\mathrm{DS}_{kl,t_k}} + \underbrace{\sum_{i\in\mathcal{P}_k/\{k\}}\sqrt{p_i}\rho_i\left[\varepsilon - t_i\right]\mathbf{o}_{il}\left[\varepsilon\right]}_{\mathrm{PC}_{kil,t_k}} \\ &+ \underbrace{\sum_{i\in\mathcal{P}_k}\sqrt{p_i}\bar{\rho}_i\left[\varepsilon - t_i\right]\mathbf{f}_{il}\left[t_i\right]}_{\mathrm{CA}_{kl,t_k}} + \mathbf{w}_l\left[t_k\right], \end{aligned} \tag{9}$$

where $\mathrm{DS}_{kl,t_k}$ denotes the desired signal, $\mathrm{PC}_{kil,t_k}$ denotes the pilot contamination, and $\mathrm{CA}_{kl,t_k}$ denotes the channel aging effect. Based on (8) and (9), if $\mathbf{R}_{kl}$ can be obtained by AP $l$, we can adopt the local MMSE aggregated channel estimation approach[4] [6], [17] to estimate the effective aggregated channel $\mathbf{o}_{kl}\left[\varepsilon\right]$ as

$$\hat{\mathbf{o}}_{kl}\left[\varepsilon\right] = \sqrt{p_k}\rho_k\left[\varepsilon - t_k\right]\mathbf{R}_{kl}\boldsymbol{\Psi}_{kl}\mathbf{z}_l\left[t_k\right], \tag{10}$$

where $\boldsymbol{\Psi}_{kl} = (\sum_{i\in\mathcal{P}_k} p_i\mathbf{R}_{il} + \sigma^2\mathbf{I}_N)^{-1}$. The estimated channel $\hat{\mathbf{o}}_{kl}\left[\varepsilon\right]$ and the channel estimation error $\tilde{\mathbf{o}}_{kl}\left[\varepsilon\right] = \mathbf{o}_{kl}\left[\varepsilon\right] - \hat{\mathbf{o}}_{kl}\left[\varepsilon\right]$ are independent random variables with the distribution as $\mathcal{CN}\left(\mathbf{0}, \boldsymbol{\Omega}_{kl}\right)$ and $\mathcal{CN}\left(\mathbf{0}, \mathbf{R}_{kl} - \boldsymbol{\Omega}_{kl}\right)$, respectively, where

$$\boldsymbol{\Omega}_{kl} \triangleq p_k\rho_k^2\left[\varepsilon - t_k\right]\mathbf{R}_{kl}\boldsymbol{\Psi}_{kl}\mathbf{R}_{kl}. \tag{11}$$

The quality of the estimated channel $\hat{\mathbf{o}}_{kl}\left[\varepsilon\right]$ is degraded by the channel aging coefficient $\rho_k\left[\varepsilon - t_k\right]$ and those UEs exploiting the same pilot at time instant $t_k$, i.e., pilot contamination. Note that when there is no channel aging, i.e., $\rho_k\left[\varepsilon - t_k\right] = 1$, the resource blocks of the considered system become the conventional block-fading model. In other words, the model in (10) is a generalization as those in [2] and [11].

## III. Uplink Data Transmission and Performance Analysis

In this section, we investigate the uplink performance of RIS-aided CF massive MIMO systems considering the RIS elements spatial correlation and channel aging. Furthermore, we derive the asymptotic closed-form expressions for analyzing the uplink SE performance by adopting MR combining. Then, compared with the SCD method, we apply the LSFD signal processing method at the CPU to further exploit the potential of the system performance.

### A. Uplink Data Transmission

We consider that the data is transmitted to all the APs by the UEs simultaneously in the uplink. Exploiting the local channel estimates, all the APs perform a local estimate of the uplink data transmission. These estimated data are then conveyed to the CPU through the dedicated fronthaul links for further joint data detection [3]. During the instants $\varepsilon \leqslant n \leqslant \tau_c$, the uplink received signal $\mathbf{y}_l\left[n\right] \in \mathbb{C}^N$ at AP $l$ can be obtained as

$$\mathbf{y}_l\left[n\right] = \sqrt{p_u}\sum_{i=1}^{K}\sqrt{\eta_i}\mathbf{o}_{il}\left[n\right]s_i\left[n\right] + \mathbf{w}_l\left[n\right], \tag{12}$$

where $p_u$ denotes the maximum uplink data transmit power and $0 \leqslant \eta_k \leqslant 1$ represents the power control coefficient, respectively. $s_i\left[n\right] \sim \mathcal{CN}\left(0,1\right)$ denotes the signal transmitted by UE $i$ and $\mathbf{w}_l\left[n\right] \sim \mathcal{CN}\left(\mathbf{0}, \sigma_u^2\mathbf{I}_N\right)$ is the receiver noise at AP $l$.

We consider that the APs locally process the uplink received data with the local combining vector $\mathbf{v}_{kl} \in \mathbb{C}^N$ which can be designed by AP $l$ for UE $k$.[5] Subsequently, the locally estimated signal $\breve{s}_{kl}\left[n\right]$ can be obtained as

$$\begin{aligned}\breve{s}_{kl}\left[n\right] =& \mathbf{v}_{kl}^{\mathrm{H}}\left[\varepsilon\right]\mathbf{y}_l\left[n\right] \\ =& \sqrt{p_u}\sum_{i=1}^{K}\mathbf{v}_{kl}^{\mathrm{H}}\left[\varepsilon\right]\mathbf{o}_{il}\left[n\right]\sqrt{\eta_i}s_i\left[n\right] + \mathbf{v}_{kl}^{\mathrm{H}}\left[\varepsilon\right]\mathbf{w}_l\left[n\right], \forall n. \end{aligned} \tag{13}$$

Here, we can represent $\mathbf{o}_{il}\left[n\right]$ by the initial state $\mathbf{o}_{il}\left[\varepsilon\right]$ in the data transmission phase as

$$\mathbf{o}_{il}\left[n\right] = \rho_i\left[n - \varepsilon\right]\mathbf{o}_{il}\left[\varepsilon\right] + \bar{\rho}_i\left[n - \varepsilon\right]\mathbf{u}_{il}\left[n\right], \tag{14}$$

[4]Based on [31], we adopt a local MMSE estimator to reduce the error of channel estimation and obtain the effective channel estimate that ages over time.

[5]Adopting the local processing at the APs can make the full use of local channel estimation to decode signals [3]. Furthermore, the CPU only requires to acquire the channel statistics instead of all the knowledge of the channel estimates, which reduces the signaling overhead required in the fronthaul [11], [32].

$$\hat{s}_k[n]=\sum_{l=1}^{L}a_{kl}^{*}[n]\breve{s}_{kl}[n]=\underbrace{\sqrt{p_u\eta_k}\rho_k[n-\varepsilon]\sum_{l=1}^{L}a_{kl}^{*}[n]\mathbb{E}\left\{\mathbf{v}_{kl}^{\mathrm{H}}[\varepsilon]\mathbf{o}_{kl}[\varepsilon]\right\}s_k[n]}_{\mathrm{DS}_{k,n}}$$
$$+\underbrace{\sqrt{p_u\eta_k}\bar{\rho}_k[n-\varepsilon]\sum_{l=1}^{L}a_{kl}^{*}[n]\mathbf{v}_{kl}^{\mathrm{H}}[\varepsilon]\mathbf{u}_{kl}[n]s_k[n]}_{\mathrm{CA}_{k,n}}+\sum_{i\neq k}^{K}\underbrace{\sqrt{p_u}\sum_{l=1}^{L}\sqrt{\eta_i}a_{kl}^{*}[n]\mathbf{v}_{kl}^{\mathrm{H}}[\varepsilon]\mathbf{o}_{il}[n]s_i[n]}_{\mathrm{UI}_{ki,n}}$$
$$+\underbrace{\sqrt{p_u\eta_k}\rho_k[n-\varepsilon]\left(\sum_{l=1}^{L}a_{kl}^{*}[n]\left(\mathbf{v}_{kl}^{\mathrm{H}}[\varepsilon]\mathbf{o}_{kl}[\varepsilon]-\mathbb{E}\left\{\mathbf{v}_{kl}^{\mathrm{H}}[\varepsilon]\mathbf{o}_{kl}[\varepsilon]\right\}\right)\right)s_k[n]}_{\mathrm{BU}_{k,n}}+\underbrace{\sum_{l=1}^{L}a_{kl}^{*}[n]\mathbf{v}_{kl}^{\mathrm{H}}[\varepsilon]\mathbf{w}_l[n]}_{\mathrm{NS}_{k,n}}. \quad (15)$$

where $\mathbf{u}_{il}[n]\sim\mathcal{CN}(\mathbf{0},\mathbf{R}_{il})$ is the independent component related to $\mathbf{o}_{il}[\varepsilon]$ and $\mathbf{o}_{il}[n]$. Then, all the APs sent the local estimates $\breve{s}_{kl}[n]$ in (13) to the CPU for signal detection. In particular, $\breve{s}_{kl}[n]$ are linearly weighted at the CPU with the weight coefficients $a_{kl}[n]\in\mathbb{C}$ to further mitigate the interference from other UEs [3]. The post-processed signal $\hat{s}_k[n]$ is given by (15) at the top of this page. $\mathrm{DS}_{k,n}$ denotes the desired signal of UE $k$, $\mathrm{CA}_{k,n}$ denotes the effect of channel aging, $\mathrm{UI}_{ki,n}$ denotes the inter-user interference, $\mathrm{BU}_{k,n}$ denotes the uncertainty of beamforming gain, and $\mathrm{NS}_{k,n}$ denotes the received noise term, respectively.

### *B. Performance Analysis*

We adopt the SCD and LSFD weighted coefficients at the CPU to study the uplink performance of the RIS-aided CF massive MIMO system, and then analyze the corresponding spatial correlations and channel aging effects.[6] Based on (15), the uplink achievable SE lower bound of UE $k$ can be expressed by adopting the use-and-then-forget (UatF) bound [3] that yeilds[7]

$$\mathrm{SE}_k=\frac{1}{\tau_c}\sum_{n=\varepsilon}^{\tau_c}\log_2\left(1+\gamma_k[n]\right), \quad (16)$$

where the effective signal-to-interference-plus-noise ratio (SINR) $\gamma_k[n]$ can be denoted as

$$\gamma_k[n]=\frac{\mathbb{E}\left\{|\mathrm{DS}_{k,n}|^2\right\}}{\mathbb{E}\left\{|\mathrm{BU}_{k,n}|^2\right\}+\mathbb{E}\left\{|\mathrm{CA}_{k,n}|^2\right\}+\sum_{i\neq k}^{K}\mathbb{E}\left\{|\mathrm{UI}_{k,n}|^2\right\}+\mathbb{E}\left\{|\mathrm{NS}_{k,n}|^2\right\}}. \quad (17)$$

**Remark 2.** *Since the closed-form expressions of the SE with MMSE combining at the AP cannot be obtained while the MR combining is simple with low computational complexity, hence, we focus on the MR combining method at the local APs to obtain the closed-form expressions of the uplink SE with* $\mathbf{v}_{kl}[\varepsilon]=\hat{\mathbf{o}}_{kl}[\varepsilon]$.

*1) Large Scale Fading Decoding:* In this case, each AP can preprocess its signal by computing the local estimates of the uplink data and then convey them to the CPU for the final signal decoding. Notice that the CPU can optimize the weight coefficient vector $\mathbf{a}_k[n]=[a_{k1}[n],\cdots,a_{kL}[n]]^{\mathrm{T}}\in\mathbb{C}^L$ to maximize the SE. Yet, the CPU can only exploit the channel statistics since it does not have any estimated knowledge of the channel acquired by the APs. It is known as the LSFD approach in massive MIMO systems [3] and the obtained key result is summarized in the following.

**Theorem 1.** *The closed-form SINR expression for the uplink SE with LSFD of UE $k$ is expressed as* (18) *at the top of the next page, where*

$$\mathbf{Z}_k\triangleq\mathrm{diag}\left(\mathrm{tr}\left(\mathbf{\Omega}_{k1}\right),\cdots,\mathrm{tr}\left(\mathbf{\Omega}_{kL}\right)\right)\in\mathbb{C}^{L\times L}, \quad (19)$$
$$\mathbf{A}_k[n]\triangleq\mathrm{diag}\left(a_{k1}[n],\cdots,a_{kL}[n]\right)\in\mathbb{C}^{L\times L}. \quad (20)$$

*Also, the non-coherent interference signal* $\mathbf{\Gamma}_{ki}$ *is denoted as*

$$\mathbf{\Gamma}_{ki}\triangleq\mathrm{diag}\left(\mathrm{tr}\left(\mathbf{\Omega}_{k1}\mathbf{R}_{i1}\right),\cdots,\mathrm{tr}\left(\mathbf{\Omega}_{k1}\mathbf{R}_{iL}\right)\right)\in\mathbb{C}^{L\times L}. \quad (21)$$

*The coherent interference is shown as*

$$\mathbf{\Lambda}_{ki}\triangleq\mathrm{diag}\left(\varpi_{ki,1},\cdots,\varpi_{ki,L}\right)\in\mathbb{C}^{L\times L}, \quad (22)$$
$$\varpi_{ki,l}\triangleq\rho_k[\varepsilon-t_k]\rho_i[\varepsilon-t_i]\sqrt{p_kp_i}\mathrm{tr}\left(\mathbf{R}_{il}\mathbf{\Psi}_{kl}\mathbf{R}_{kl}\right). \quad (23)$$

*Finally, the noise at the CPU is shown as*

$$\mathbf{\Xi}_k\triangleq\mathrm{diag}\left(\mathrm{tr}\left(\mathbf{\Omega}_{k1}\right),\cdots,\mathrm{tr}\left(\mathbf{\Omega}_{kL}\right)\right)\in\mathbb{C}^{L\times L}. \quad (24)$$

*Proof:* The proof is given in Appendix A. ■

Indeed, without the RIS, the closed-form SINR (18) in Theorem 1 degenerates to the results in [27]. Furthermore, we notice that the LSFD coefficient vector $\mathbf{a}_k[n]$ is different for different time instant $n$ while the CPU can optimize $\mathbf{a}_k[n]$ to maximize the effective SINR in (18). In the following, we introduce a corollary for the optimal choice of the LSFD coefficient.

[6]Note that the LSFD can maximize the SE of UE $k$ but at the cost of high computational complexity [3]. In contrast, the SCD has a lower computational complexity but with some performance loss. Both decoding methods are typical in CF massive MIMO syetems [33].

[7]Note that to achieve channel hardening and favorable propagation [34], the number of antennas needs to approach infinity. Considering this, we adopt the UatF bound to derive the closed-form SINR expressions, which yields a lower bound of the ergodic SE.

$$\gamma_k^{\mathrm{LSFD}}[n]=\frac{\rho_k^2[n-\varepsilon]\,p_u\eta_k\left|\mathrm{tr}\left(\mathbf{A}_k^{\mathrm{H}}[n]\,\mathbf{Z}_k\right)\right|^2}{p_u\sum\limits_{i=1}^{K}\eta_i\mathrm{tr}\left(\mathbf{A}_k^{\mathrm{H}}[n]\,\mathbf{\Gamma}_{ki}\mathbf{A}_k[n]\right)+p_u\sum\limits_{i\in\mathcal{P}_k\setminus\{k\}}\rho_i^2[n-\varepsilon]\,\eta_i\left|\mathrm{tr}\left(\mathbf{A}_k^{\mathrm{H}}[n]\,\mathbf{\Lambda}_{ki}\right)\right|^2+\sigma_u^2\mathrm{tr}\left(\mathbf{A}_k^{\mathrm{H}}[n]\,\mathbf{\Xi}_k\mathbf{A}_k[n]\right)}. \tag{18}$$

$$\gamma_k^{\mathrm{SCD}}[n]=\frac{\rho_k^2[n-\varepsilon]\,p_u\eta_k\left|\mathrm{tr}\left(\mathbf{Z}_k\right)\right|^2}{p_u\sum\limits_{i=1}^{K}\eta_i\mathrm{tr}\left(\mathbf{\Gamma}_{ki}\right)+p_u\sum\limits_{i\in\mathcal{P}_k\setminus\{k\}}\rho_i^2[n-\varepsilon]\,\eta_i\left|\mathrm{tr}\left(\mathbf{\Lambda}_{ki}\right)\right|^2+\sigma_u^2\mathrm{tr}\left(\mathbf{\Xi}_k\right)}. \tag{27}$$

**Corollary 1.** *The optimal LSFD coefficient for maximizing the SINR is expressed as*

$$\mathbf{a}_k[n]=\left(p_u\sum_{i=1}^{K}\eta_i\mathbf{\Gamma}_{ki}-p_u\sum_{i\in\mathcal{P}_k\setminus\{k\}}\eta_i\rho_i^2[n-\varepsilon]\mathbf{\Lambda}_{ki}\mathbf{\Lambda}_{ki}^{\mathrm{H}}+\sigma^2\mathbf{\Xi}_k\right)^{-1}\mathbf{b}_k, \tag{25}$$

*where* $\mathbf{b}_k=\mathrm{diag}\left(\mathbf{Z}_k\right)$. *Then, the maximum SE in* (16) *can be realized with SINR* $\gamma_k^{\mathrm{LSFD}}$ *as*

$$\gamma_k^{LSFD}[n]=p_u\eta_k\rho_k^2[n-\varepsilon]\,\mathbf{b}_k^H\left(p_u\sum_{i=1}^{K}\eta_i\mathbf{\Gamma}_{ki}-p_u\sum_{i\in\mathcal{P}_k\setminus\{k\}}\eta_i\rho_i^2[n-\varepsilon]\,\mathbf{\Lambda}_{ki}\mathbf{\Lambda}_{ki}^H+\sigma^2\mathbf{\Xi}_k\right)^{-1}\mathbf{b}_k. \tag{26}$$

*Proof:* By following the standard results in [4], (25) and (26) can be easily derived and therefore omitted. ■

As the channel aging coefficient $\rho_i[n-\varepsilon]$ decreases, the weight coefficient $a_{kl}[n]$ in (25) decreases accordingly, which means that the corresponding signal impact is reduced to compensate for the impact of channel aging when the channel aging becomes serious. Meanwhile, from Corollary 1 we can observe that the increase of $\rho_k[n-\varepsilon]$ leads to the increase of SINR in (26). As such, channel aging is detrimental to the system performance. The computational complexities for complex-valued multiplications of the LSFD are $\mathcal{O}\left(\frac{1}{3}L^3+\left(K+\frac{3}{2}\right)L^2+\frac{13}{6}L\right)$. Obviously, although the LSFD can achieve better performance by optimizing the weight coefficient, its computational complexity is high, especially when the number of APs is large.

On the other hand, let us consider the application of the SCD at the CPU that enjoys a lower computational complexity but at the expense of some performance loss.

*2) Simple Centralized Decoding:* In this case, the received signals at each AP are processed with MR combining, then are all sent to the CPU for further processing with SCD [3]. Actually, it is a special case of LSFD and the coefficient is written as $\mathbf{a}_k=[1,\cdots,1]^T\in\mathbb{C}^{L\times 1}$.

**Corollary 2.** *The SINR* $\gamma_k^{\mathrm{SCD}}$ *is denoted as* (27) *at the top of this page.*

**Remark 3.** *It is noted that in both* (18) *and* (27)*, the channel aging affects both the denominator and numerator of the SINR through* $\rho_k[n-\varepsilon]$. *However, it is obvious that when* $\rho_k[n-\varepsilon]\to 0$*, i.e., the impact of the channel aging becomes extremely serious, the denominator decreases and the* $\mathrm{SINR}\to 0$. *Also, if we assume that the number of AP antennas* $N\to\infty$*, then we can obtain that* $\mathbf{R}_{kl}\approx\mathbf{R}_{kl,d}$ *such that* $\mathrm{tr}\left(\mathbf{\Omega}_{kl}\right)=\rho_k^2[\lambda-t_k]\,p_k\beta_{kl,d}^2\Psi_{kl}N$*, where* $\Psi_{kl}=(\sum\limits_{i\in\mathcal{P}_k}p_i\beta_{il}+\sigma^2)^{-1}$. *Then,* (18) *and* (27) *can be rewritten in the form of* $\gamma_k^u=\dot{x}/(\dot{y}+\dot{z}/N)$*, where* $\dot{x}$ *denotes the desired signal,* $\dot{y}$ *and* $\dot{z}$ *denote the inter-users interference and the noise, respectively. In this case, we can find that the uplink SINR of UE* $k$ *is a monotonicity increasing function of* $N$.

## IV. Downlink Data Transmission

In this section, we apply the same framework as the uplink to study the SE performance problem in the downlink. By considering the impacts of channel aging and spatial correlations, we derive the downlink achievable SE closed-form expressions. Subsequently, we introduce a practical FPC to further improve the performance of the considered system.

### A. Downlink Data Transmission and Performance Analysis

As shown in Fig. 2, the time instants $\tau_c-\tau_p$ are adopted for downlink data transmission in each downlink resource block. We assume that the RIS-aided CF massive MIMO system adopt the coherent joint transmission and all the APs transmit the same data symbols to each UE. By exploiting the MR precoding, the downlink transmitted signal from AP $l$ at $n$th time instant can be denoted as

$$\mathbf{x}_l[n]=\sqrt{p_d}\sum_{i=1}^{K}\hat{\mathbf{o}}_{il}[\varepsilon]\sqrt{\mu_{il}}s_i^d[n], \tag{28}$$

where $p_d$ represents the maximum transmission power for each AP in the downlink, and $0\leqslant\mu_{il}\leqslant 1$ denotes the power control coefficient. $s_i^d[n]\sim\mathcal{CN}(0,1)$ denotes the signal transmitted from the APs to UE $i$ and $\mathbb{E}\left\{s_i^d[n]\,s_k^d[n]\right\}=0,\forall i\neq k$. Based on (14), the received signal sent from all the APs at UE $k$ at $n$th time instant is given by (29) at the top of the next page, where $\mathrm{DS}_{k,n}^d$ denotes the downlink desired signal, $\mathrm{CA}_{k,n}^d$ denotes the channel aging, $\mathrm{UI}_{ki,n}^d$ denotes the inter-user interference, and $w_k^d[n]\sim\mathcal{CN}\left(0,\sigma_d^2\right)$ denotes the noise.

**Theorem 2.** *The closed-form expression for the downlink SE of UE* $k$ *is expressed as*

$$SE_k^d=\frac{1}{\tau_c}\sum_{n=\varepsilon}^{\tau_c}\log_2\left(1+\gamma_k^d[n]\right), \tag{30}$$

$$y_k^d[n] = \sum_{l=1}^{L} \mathbf{o}_{kl}^{\mathrm{H}}[n]\,\mathbf{x}_l[n] + w_k[n] = \underbrace{\sqrt{p_d}\rho_k[n-\varepsilon]\sum_{l=1}^{L}\sqrt{\mu_{kl}}\mathbf{o}_{kl}^{\mathrm{H}}[\varepsilon]\hat{\mathbf{o}}_{kl}[\varepsilon]\,s_k^d[n]}_{\mathrm{DS}_{k,n}^d}$$
$$+ \underbrace{\sqrt{p_d}\sum_{l=1}^{L}\sum_{i\neq k}^{K}\sqrt{\mu_{il}}\mathbf{o}_{kl}^{\mathrm{H}}[n]\hat{\mathbf{o}}_{il}[\varepsilon]s_i^d[n]}_{\mathrm{UI}_{ki,n}^d} + \underbrace{\sqrt{p_d}\bar{\rho}_k[n-\varepsilon]\sum_{l=1}^{L}\sqrt{\mu_{kl}}\mathbf{u}_{kl}^{\mathrm{H}}[n]\hat{\mathbf{o}}_{kl}[\varepsilon]\,s_k^d[n]}_{\mathrm{CA}_{k,n}^d} + w_k^d[n]. \tag{29}$$

*where $\gamma_k^d[n]$ is expressed as* (31) *at the top of the next page. The closed-form expression of SINR in* (30) *can be further computed and represented as (32) at the top of the next page, where $\widetilde{\mathbf{\Omega}}_{kil} = \sqrt{p_i p_k}\rho_i[\varepsilon - t_i]\,\rho_k[\varepsilon - t_k]\,\mathbf{R}_{il}\mathbf{\Psi}_{kl}\mathbf{R}_{kl}$.*

*Proof:* The proof of (32) can be derived by following the similar steps as Theorem 1. ∎

**Remark 4.** *Note that without the cascaded channel of RIS, Theorem 2 is degraded into [27, Eq. (35)]. Besides, focusing on the impact of channel aging, the SINR in (32) can be rewritten in the form of $\gamma_k^d = \dot{a}\Big/\left(\dot{b} + \dot{\zeta}\dot{c}\right)$, where $\dot{\zeta} \triangleq 1/\rho_k^2[n-\varepsilon]$, $\dot{a}$ denotes the desired signal, $\dot{b}$ and $\dot{c}$ are mainly dependent on the inter-users interference and the noise, respectively. $\dot{a}$, $\dot{b}$, and $\dot{c}$ are positive constants. Thus, we can find that the downlink SINR of UE $k$ is a monotonicity increasing function of the temporal correlation coefficient $\rho_k[n-\varepsilon]$ which reveals that the existence of channel aging reduces the downlink performance of UEs.*

### *B. Downlink Fractional Power Control*

For the downlink data transmission, we focus on the UEs fairness and aim to improve the QoS for the UEs that have poor connection strength with APs. In practice, in CF massive MIMO systems, the system performance is limited by the near-far effects [2] which still exist in the considered system. To tackle this issue, we extend the power control policy in [27] to the considered system. Specifically, we utilize the estimated channel information and obtain the FPC coefficients to equalize the path gain as

$$\mu_{kl} = \frac{\beta_k^{-1}}{\sum_{i=1}^{K}\mathrm{tr}\left(\mathbf{\Omega}_{il}\right)\beta_i^{-1}},\ l = 1,\ldots,L, k = 1,\ldots,K, \tag{33}$$

where $\beta_k = \sum_{l=1}^{L}\mathrm{tr}\left(\mathbf{R}_{kl}\right)\Big/L$ represents the average connection strength between UE $k$ and all APs, while $\mathrm{tr}\left(\mathbf{\Omega}_{il}\right)$ introduces the effects of channel aging.

**Remark 5.** *Note that when channel aging is severe, $tr\left(\mathbf{\Omega}_{il}\right)$ becomes small such that the power coefficient increases to improve UEs performance. Also, from* (33)*, it can be observed that when $\beta_k$ is small, it means that the average channel quality from user $k$ to all APs is poor. In such cases, the power coefficient $\mu_{kl}$ allocated to user $k$ is increased to improve performance.*

## V. Numerical Results and Discussion

We assume that all the APs and UEs are randomly distributed within the $500\ \mathrm{m} \times 500\ \mathrm{m}$ area, respectively. Meanwhile, each RIS is deployed at a distance of $5\ \mathrm{m}$ from the corresponding AP. Also, we set the carrier frequency $f_c = 2$ GHz. In addition, the length of each coherence block is $\tau_c = 200$ and $\tau_p = 8$ are adopted for pilot transmission.

For the path loss, we take AP $l$-UE $k$ as an example and we adopt a three-slope propagation model [5] to compute the path loss $\beta_{kl,d}^o$. We obtain $\mathbf{R}_{kl,d}$ from [27] with the angular standard deviation (ASD) denoting the correlation strength, which is determined by the position and angle of the transmitter and receiver antennas. Notably, we consider the direct links are under harsh propagation conditions due to the presence of large obstacles and the obstacle fading coefficient $\alpha$ is denoted as $\beta_{kl,d} = \beta_{kl,d}^o \times 10^{-\alpha}$ which represents the connection strength of the direct link from the APs to the UEs. Without loss of generality, we assume the pilot transmit power $p_k = 20\,\mathrm{dBm}, \forall k$. Meanwhile, the uplink and the downlink maximum transmission power are $p_u = 20\,\mathrm{dBm}$ and $p_d = 23\,\mathrm{dBm}$, respectively. Finally, the noise power is $\sigma^2 = -96\,\mathrm{dBm}$.

### *A. The Length of Resource Blocks*

Fig. 3 shows the average SE per UE of the uplink with LSFD or SCD and the downlink with FPC in RIS-aided CF massive MIMO system in the first $500$ time instant indices. Here, we assume that the resource block length is longer than 500. We notice that the first zero position appears at $n = 395$ and $n = 200$ with the Doppler shift $f_D T_s$ increasing from 0.001 to 0.002, corresponding to the UEs' mobility ranged from $15$ m/s to $30$ m/s. It means that as the UE movement speed increases, the communication performance is degraded. In particular, for a sufficiently high UE's mobility, the lower bound of the SE derived in (18), approaches zero due to the use of UatF bound. Meanwhile, the peaks of the fluctuations become smaller with increases of the time instant index. Hence, it is necessary to reasonably design the resource block length to reduce the channel aging effect. Considering that, in Fig. 4, we evaluate the sum SE (expressed as $\mathrm{SE}_{\mathrm{sum}} = \sum_{k=1}^{K}\left(\frac{1}{2}\mathrm{SE}_k^{\mathrm{LSFD}} + \frac{1}{2}\mathrm{SE}_k^d\right)$) with different resource block length $\tau_c$ against the value of $f_D T_s$. It is clear that as $\tau_c$ increases, the sum SE drops faster and RIS can provide significant performance gains. To further reduce the impact of channel aging, we restrict the resource block $\tau_c$ such that

$$\gamma_k^d[n] = \frac{\rho_k^2[n-\varepsilon]\, p_d \sum_{l=1}^{L} \mu_{kl} \left| \mathbb{E}\left\{ \mathbf{o}_{kl}^{\mathrm{H}}[\varepsilon]\, \hat{\mathbf{o}}_{kl}[\varepsilon] \right\} \right|^2}{p_d \sum_{i=1}^{K} \sum_{l=1}^{L} \mu_{il} \mathbb{E}\left\{ \left| \mathbf{o}_{kl}^{\mathrm{H}}[\varepsilon]\, \hat{\mathbf{o}}_{il}[\varepsilon] \right|^2 \right\} - \rho_k^2[n-\varepsilon]\, p_d \sum_{l=1}^{L} \mu_{kl} \left| \mathbb{E}\left\{ \mathbf{o}_{kl}^{\mathrm{H}}[\varepsilon]\, \hat{\mathbf{o}}_{kl}[\varepsilon] \right\} \right|^2 + \sigma_d^2}. \tag{31}$$

$$\gamma_k^d[n] = \frac{\rho_k^2[n-\varepsilon]\, p_d \left| \sum_{l=1}^{L} \sqrt{\mu_{kl}} \mathrm{tr}\left( \mathbf{\Omega}_{kl} \right) \right|^2}{p_d \sum_{i=1}^{K} \sum_{l=1}^{L} \mu_{il} \mathrm{tr}\left( \mathbf{\Omega}_{il} \mathbf{R}_{kl} \right) + \rho_k^2[n-\varepsilon]\, p_d \sum_{i \in \mathcal{P}_k \setminus \{k\}} \left| \sum_{l=1}^{L} \sqrt{\mu_{il}} \mathrm{tr}\left( \bar{\mathbf{\Omega}}_{kil} \right) \right|^2 + \sigma_d^2}. \tag{32}$$

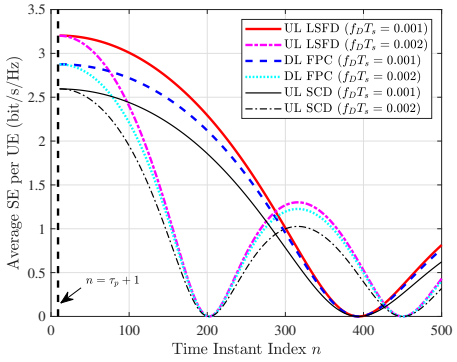


Fig. 3: Average uplink and downlink SE against different values of $f_D T_s$ with time instant index ($L = 60$, $K = 10$, $N = 2$, $M = 64$, $\tau_p = 8$, $d_{\mathrm{V}} = d_{\mathrm{H}} = \frac{1}{2}\lambda$, $\alpha = 0$).

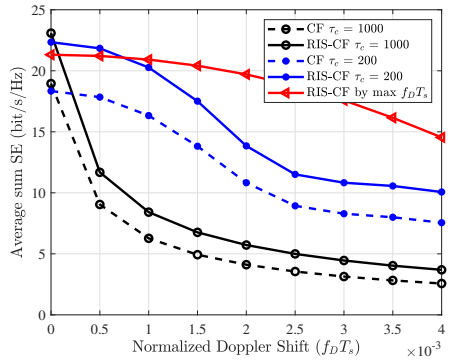


Fig. 4: Average sum SE against different values of $f_D T_s$ under different lengths design of the resource block ($L = 60$, $K = 10$, $N = 2$, $M = 64$, $\tau_p = 8$, $d_{\mathrm{V}} = d_{\mathrm{H}} = \frac{1}{2}\lambda$, $\alpha = 0$).

it is less than the value $n$ of the first zero point in Fig. 3. More specifically, we adopt the maximum Doppler shift, i.e., $f_D T_s = 0.004$ in Fig. 4 to calculate the value of the first zero point. As shown in Fig. 4, with the adjusted practical channel aging-aware resource block design, the sum SE tends to be more stable in the considered range of Doppler frequency shift as the resource blocks become shorter to mitigate the impacts caused by channel aging.

Fig. 5 shows the average sum SE (expressed as $\mathrm{SE}_{\mathrm{sum}} = \sum_{k=1}^{K} \left( \frac{1}{2}\mathrm{SE}_k^{\mathrm{LSFD}} + \frac{1}{2}\mathrm{SE}_k^d \right)$) against different lengths of the resource block $\tau_c$ under different $f_D T_s$ with/without a training phase before the downlink transmission. We find that in the

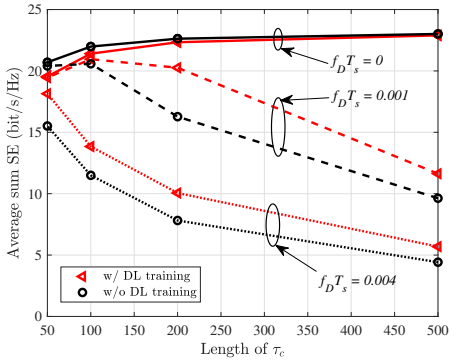


Fig. 5: Average sum SE against different lengths of resource block $\tau_c$ under different $f_D T_s$ with/without training phase before downlink transmission ($L = 60$, $K = 10$, $N = 2$, $M = 64$, $\tau_p = 8$, $d_{\mathrm{V}} = d_{\mathrm{H}} = \frac{1}{2}\lambda$, $\alpha = 0$).

absence of channel aging, i.e., $f_D T_s = 0$, performing training only on the uplink frame structure can achieve better performance than that on both the uplink and downlink. However, when the channel aging becomes severe, i.e., $f_D T_s = 0.004$, the advantage of introducing an extra pilot training phase before the downlink data transmission is highlighted. Specifically, when $f_D T_s = 0.001$, the average sum SE first increases and then decreases with the increases in $\tau_c$. However, the introduction of a training phase before the downlink data transmission can alleviate the rate of performance degradation. These findings underscore the necessity of incorporating extra training periods before the downlink data transmission, especially when channel aging is severe and the length of a resource block is long.

The average uplink SE per UE for CF and RIS-aided CF massive MIMO systems against the number of $\tau_p$ is shown in Fig. 6. It is clear that when $\tau_p < K$, increasing $\tau_p$ can improve the system performance of the above two systems. Meanwhile, with $\tau_p > K$, the average SE decreases as $\tau_p$ increases because of the pilot redundancy occupying the data transmission block dominating the resource consumption. Besides, we find that the length of the pilot has a more significant impact on the RIS-aided CF massive MIMO system than the CF massive MIMO system since the cascaded link introduced by RIS brings additional channel aging effects and pilot contamination. This reveals that it is particularly important to ensure the number of $\tau_p$ as close as possible to the number of UE $K$ to suppress the pilot contamination

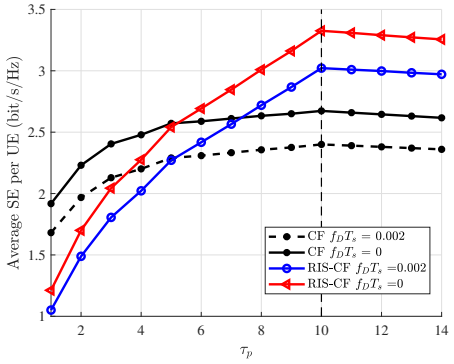


Fig. 6: Average uplink SE per UE for CF and RIS-aided CF massive MIMO system against $\tau_p$ with different values of $f_DT_s$ under LSFD ($L = 60$, $K = 10$, $N = 2$, $M = 64$, $d_{\mathrm{V}} = d_{\mathrm{H}} = \frac{1}{2}\lambda$, $\alpha = 0$).

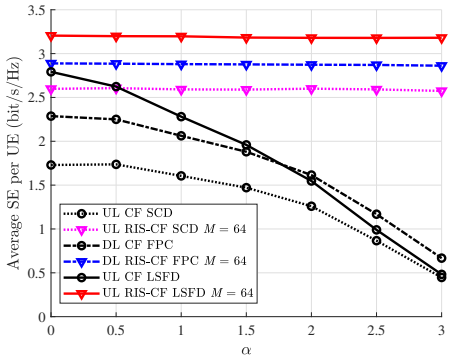


Fig. 7: Average uplink and downlink SE for CF and RIS-aided CF massive MIMO system against $\alpha$ ($L = 60$, $K = 10$, $N = 2$, $\tau_p = 8$, $d_{\mathrm{V}} = d_{\mathrm{H}} = \frac{1}{2}\lambda$, $f_DT_s = 0.001$).

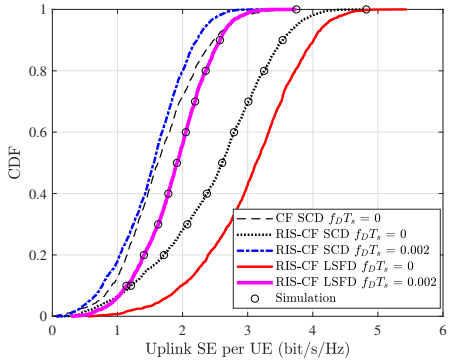


Fig. 8: CDF of uplink SE per UE against the number of $M$ with SCD and LSFD ($L = 60$, $K = 10$, $N = 2$, $\tau_p = 8$, $d_{\mathrm{V}} = d_{\mathrm{H}} = \frac{1}{2}\lambda$, $\alpha = 0$).

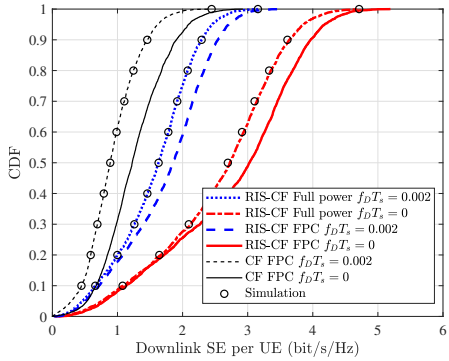


Fig. 9: CDF of downlink SE per UE against different values of $f_DT_s$ with full power and FPC ($L = 60$, $K = 10$, $N = 2$, $M = 100$, $\tau_p = 8$, $d_{\mathrm{V}} = d_{\mathrm{H}} = \frac{1}{2}\lambda$, $\alpha = 0$).

caused by channel aging for RIS-aided CF massive MIMO systems.

### *B. Spectral Efficiency Analysis*

Fig. 7 shows the average SE of the uplink with LSFD or SCD and the downlink with FPC as a function of the obstacle fading coefficient $\alpha$. We find that in both the uplink and downlink data transmission when the direct link becomes weak or even obscured, the performance of the RIS-aided CF massive MIMO system drops slowly, while that of the CF system drops rapidly and finally approaches 0.5 bit/s/Hz. This indicates the important role of RIS in the case of serious link occlusion even in mobility scenarios. Furthermore, we introduce LSFD in the CPU to explore the potential of the system performance. It is clear that RIS-aided CF massive MIMO system performance is always better than CF mMIMO system with LSFD. These reveal that when the CF massive MIMO system has serious obstructions, deploying RIS is an effective solution to improve the system performance.

Fig. 8 compares the cumulative distribution function (CDF) of the average uplink SE per UE for the RIS-aided CF massive MIMO system against different numbers of $M$ with SCD or LSFD, respectively. We illustrate the CDF of the uplink SE by adopting Monte-Carlo simulations and the proposed analytical framework. We observe that the user performance in the RIS-aided CF system adopting SCD closely matches that of the CF system without channel aging. It reveals that the introduction of RIS can effectively compensate for the performance degradation in CF systems caused by channel aging. Also, compared with SCD cooperation at the CPU, the LSFD achieves a performance improvement of 91% and 68% at $f_DT_s = 0$ and $f_DT_s = 0.002$ at 95% of the SE, respectively. Besides, by comparing the RIS-aided CF system with channel aging adopting the LSFD method and the RIS-aided CF system without channel aging adopting SCD, we find that for 95%-likely per-user SE point, even in the presence of channel aging, the implementation of the LSFD method still achieves performance improvement. Therefore, LSFD can provide better performance compared to SCD in RIS-aided CF massive MIMO systems. However, as channel aging becomes severe, the improvement slows down with respect to SCD.

The CDF of the average downlink SE per UE for RIS-aided CF massive MIMO systems against different values of $f_DT_s$ under different power control schemes is shown in Fig. 9. We utilize the Monte-Carlo simulations to confirm the accuracy of the downlink-derived analysis in (31). It is clear that RIS can effectively compensate for a substantial portion of the performance loss caused from channel aging. Also, compared with full power transmission, the practical FPC can

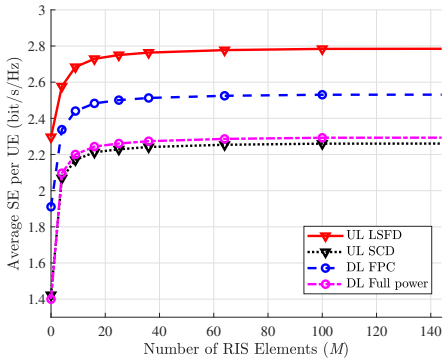


Fig. 10: Average uplink and downlink SE per UE for RIS-aided CF massive MIMO system against different number of RIS elements $M$ ($L = 60$, $K = 10$, $N = 2$, $\tau_p = 8$, $d_{\mathrm{V}} = d_{\mathrm{H}} = \frac{1}{2}\lambda$, $\alpha = 0$, $f_D T_s = 0.001$).

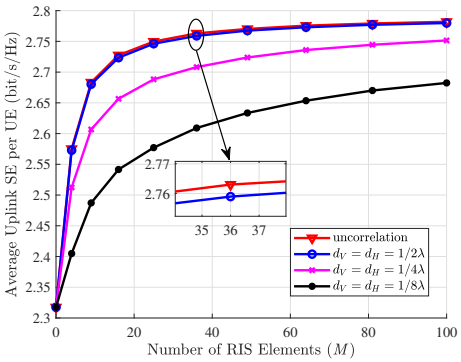


Fig. 11: Average uplink SE per UE for RIS-aided CF massive MIMO system versus RIS elements $M$ under different RIS elements spatial correlation ($L = 60$, $K = 10$, $N = 2$, $\tau_p = 8$, $\alpha = 0$, $f_D T_s = 0.001$).

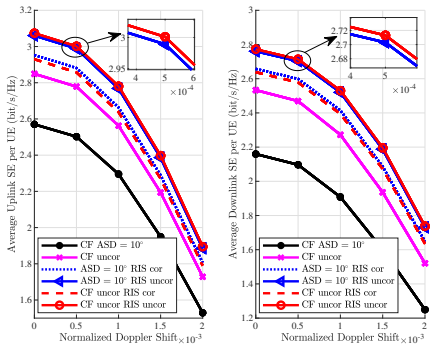


Fig. 12: Average uplink SE per UE against different $f_D T_s$ with spatial correlation of RIS elements and AP antennas over the LSFD and FPC ($L = 60$, $K = 10$, $N = 2$, $M = 64$, $\tau_p = 8$, $\alpha = 0$).

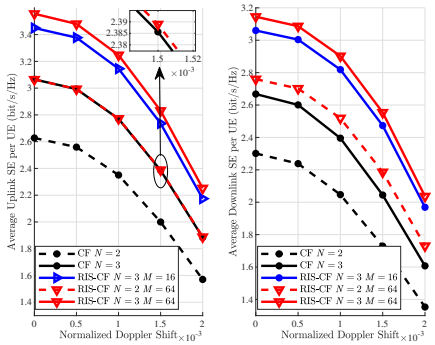


Fig. 13: Average uplink and downlink SE per UE against different $f_D T_s$ with different number of RIS elements and AP antennas over the LSFD and FPC ($L = 60$, $K = 10$, $\tau_p = 8$, $d_{\mathrm{V}} = d_{\mathrm{H}} = \frac{1}{2}\lambda$, $\alpha = 0$).

significantly improve the SE for UEs with poor performance. Besides, we notice that increasing $f_D T_s$ from 0 to 0.002 leads to the gain caused by the FPC scheme over the full-power one is 13% and 11% at 50% of SE, respectively. It reveals that even with severe channel aging, FPC is still a satisfactory choice for balancing the UEs' performance in the considered systems.

Fig. 10 shows the uplink and downlink average SE per UE for the RIS-aided CF mMIMO system against different number of RIS elements under different combining schemes. It is clear that both the uplink SE with SCD and LSFD combining, as well as the downlink SE with FPC and full power transmission increase with increasing number of RIS elements $M$. In particular, the performance improvement of LSFD is more significant. Indeed, the LSFD can exploit the global knowledge of the channel statistics in the entire network to optimize the weight coefficients that can effectively mitigate multiuser interference. This approach is effective for the RIS to compensate for performance degradation due to channel aging. Notably, compared with $M = 36$, having $M = 144$ only offers a marginal performance gain. It reveals that continuously increasing the number of RIS elements with non-adaptive phase shifts under channel aging is not cost-effective, even when employing LSFD.

Fig. 11 shows the average uplink SE per UE for the RIS-aided CF massive MIMO system versus the number of RIS elements $M$ under different RIS elements spatial correlations. $d_H = d_V = \frac{1}{8}\lambda, \frac{1}{4}\lambda, \frac{1}{2}\lambda$ denote different spatial correlations of RIS elements, $\mathbf{R} = \mathbf{I}_M$ denotes the case of no spatial correlation. Note that the RIS elements' spatial correlation has a negative effect on the uplink SE which degrades the effectiveness of passive beamforming of the RIS. Furthermore, when $d_H = d_V = \frac{1}{2}\lambda$, its SE performance approaches that of the ideal one. In particular, when the number of RIS elements $M$ varies from 16 to 100, the loss of average SE for strong spatial correlation (i.e., $d_V = \frac{1}{8}\lambda$) and weak correlation is 0.181 bit/s/Hz and 0.098 bit/s/Hz, respectively. Thus, separating the neighboring RIS elements by half a wavelength distance is important. Yet, when the number of RIS elements is sufficiently large, the influence of spatial correlation will be weakened in RIS-aided CF mMIMO systems under channel aging.

Fig. 12 illustrates the average uplink SE per UE against different $f_D T_s$ when considering the spatial correlation of RIS elements and AP antennas with the LSFD scheme. Here, the variables $\mathbf{R}_{kl,d} = \beta_{kl,d}\mathbf{I}_N$ and ASD $= 10°$ represent the uncorrelated and strong spatial correlation of AP antennas,

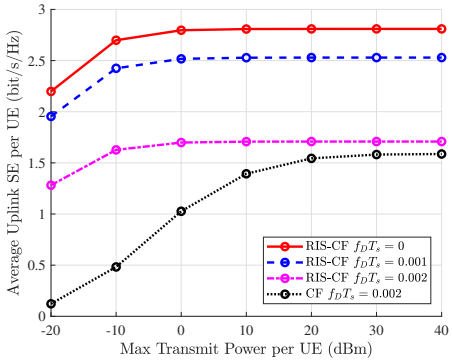


Fig. 14: Average uplink SE per UE against different UE maximum transmit power with different values of $f_D T_s$ over the LSFD ($L = 60$, $K = 10$, $N = 2$, $M = 16$, $\tau_p = 8$, $d_{\mathrm{V}} = d_{\mathrm{H}} = \frac{1}{2}\lambda$, $\alpha = 0$).

respectively. Additionally, $\mathbf{R} = \mathbf{I}_M$ and $d_V = \frac{1}{8}\lambda$ denote the uncorrelated and the strong spatial correlation of RIS elements, respectively. It is important to note that the presence of either type of correlation mentioned above individually jeopardizes system performance. Furthermore, in the RIS-aided CF mMIMO system, the impact of spatial correlation between AP antennas becomes less significant compared to the conventional CF system. This phenomenon can be attributed to the mutual coupling of correlations, where the spatial correlation of AP antennas can have a positive impact on system performance due to its interaction with the RIS correlation, which originally has a negative impact. This observation reveals that deploying RIS can effectively mitigate the negative effects caused by spatial correlation between AP antennas.

Fig. 13 displays the average uplink and downlink SE per UE for various $f_D T_s$ considering different numbers of RIS elements and AP antennas with the LSFD and FPC schemes. From the graph, it is evident that both uplink and downlink performance improves with an increase in the number of RIS elements or AP antennas. Specifically, in the RIS-aided CF massive MIMO system,the uplink performance with $N = 2$ antennas at the AP and $M = 64$ elements at the RIS surpasses that of the CF massive MIMO system with $N = 3$ antennas at the AP. Moreover, the improvement in downlink performance is even more substantial. Therefore, when the hardware resources for AP antennas are limited, deploying cost-effective RIS can still yield the expected performance enhancements, even in the presence of channel aging.

Fig. 14 shows the average uplink SE per UE against different UE maximum transmit powers with different values of $f_D T_s$ over the LSFD. We note that as the UE's maximum transmit power increases, the SE increases with diminishing returns and becomes saturated eventually at sufficiently high transmit power. Also, after deploying multiple RISs, the system requires a lower power consumption than the CF system to achieve the corresponding SE upper bound. It reveals that deploying RIS can lead to energy savings while still achieving excellent performance.

## VI. Conclusions

In this paper, we investigated the uplink and downlink performance of RIS-aided CF massive MIMO systems with channel aging over spatially correlated channels. For the uplink, we considered the MR combining at the APs and the SCD or LSFD cooperations at the CPU. As for the downlink, we adopted the MR signal precoding at the APs and proposed the practical FPC method. In particular, we derived the uplink and downlink SE closed-form expressions and quantified the impact of channel aging for the considered system. Our results showed that in both mobile and static scenarios, the RIS-aided CF massive MIMO system performs better than the CF system in both uplink and downlink. By contrast, when the channel of the direct link is in deep fade, the above performance improvement is more significant. In practice, designing the RIS element spacing to be half a wavelength can effectively minimize the spatial correlation, thereby reducing the impact of channel aging. Also, RIS can reduce the overhead of AP antennas number and couple the spatial correlation of AP antennas to reduce the impact of the latter. Furthermore, the results show that even with severe channel aging, the channel aging-aware FPC is still a satisfactory choice for balancing the UEs' performance. Meanwhile, for practical applications in mobility scenarios of RIS-aided CF massive MIMO systems, we proposed the channel aging aware resource block design scheme to improve and stabilize the sum SE. In conclusion, deploying RISs in CF massive MIMO scenarios with mobile UEs can achieve satisfactory system performance gains due to their ability to compensate for system performance degradation caused by channel aging. In the future, we will design RIS phase shifts for Rician fading channels based on channel aging to explore the potential of RISs and further improve system performance.

## Appendix A
## Proof of Theorem 1

We begin with the term $\mathbb{E}\left\{\left|\mathrm{DS}_{k,n}\right|^2\right\} = p_u \eta_k \rho_k^2 [n-\varepsilon] \left| \sum_{l=1}^{L} a_{kl}^* [n] \, \mathbb{E}\left\{\hat{\mathbf{o}}_{kl}^{\mathrm{H}} [\varepsilon] \, \mathbf{o}_{kl} [\varepsilon]\right\} \right|^2$ in the numerator. Based on the feature of the MMSE estimation, $\hat{\mathbf{o}}_{il} [\varepsilon]$ and $\tilde{\mathbf{o}}_{il} [\varepsilon]$ are independent and we can obtain

$$\begin{aligned} \mathbb{E}\left\{\hat{\mathbf{o}}_{kl}^{\mathrm{H}} [\varepsilon] \, \mathbf{o}_{kl} [\varepsilon]\right\} &= \mathbb{E}\left\{\hat{\mathbf{o}}_{kl}^{\mathrm{H}} [\varepsilon] \left(\hat{\mathbf{o}}_{kl} [\varepsilon] + \tilde{\mathbf{o}}_{kl} [\varepsilon]\right)\right\} \\ &= \rho_k^2 [\varepsilon - t_k] \, p_k \mathrm{tr}\left(\mathbf{R}_{kl} \boldsymbol{\Psi}_{kl} \mathbf{R}_{kl}\right). \end{aligned} \quad (34)$$

Applying the results in (34) to the numerator, we can obtain

$$\mathbb{E}\left\{\left|\mathrm{DS}_{k,n}\right|^2\right\} = p_u \eta_k \rho_k^2 [n-\varepsilon] \left| \sum_{l=1}^{L} a_{kl}^* [n] \, \mathrm{tr}\left(\boldsymbol{\Omega}_{kl}\right) \right|^2. \quad (35)$$

Then, we calculate the denominator terms of (18). For tractability, we first compute $\mathbb{E}\left\{\hat{\mathbf{o}}_{kl}^{\mathrm{H}} [\varepsilon] \, \mathbf{o}_{il} [\varepsilon]\right\}$. For the case $i \notin \mathcal{P}_k$, we have $\mathbb{E}\left\{\hat{\mathbf{o}}_{kl}^{\mathrm{H}} [\varepsilon] \, \mathbf{o}_{il} [\varepsilon]\right\} = 0$. As for case $i \in \mathcal{P}_k$, we can obtain

$$\begin{aligned} &\mathbb{E}\left\{\hat{\mathbf{o}}_{kl}^{\mathrm{H}} [\varepsilon] \, \mathbf{o}_{il} [\varepsilon]\right\} \\ &= \rho_k [\varepsilon - t_k] \sqrt{p_k} \rho_i [\varepsilon - t_k] \sqrt{p_i} \mathrm{tr}\left(\mathbf{R}_{il} \boldsymbol{\Psi}_{kl} \mathbf{R}_{kl}\right). \end{aligned} \quad (36)$$

$$\begin{aligned}\mathbb{E}\left\{\left|\mathrm{BU}_{k,n}\right|^2\right\} &= \mathbb{E}\left\{\left|\sqrt{\eta_k p_u}\rho_k\left[n-\varepsilon\right]\left(\sum_{l=1}^{L} a_{kl}^*\left[n\right]\left(\hat{\mathbf{o}}_{kl}^{\mathrm{H}}\left[\varepsilon\right]\mathbf{o}_{kl}\left[\varepsilon\right]-\mathbb{E}\left\{\hat{\mathbf{o}}_{kl}^{\mathrm{H}}\left[\varepsilon\right]\mathbf{o}_{kl}\left[\varepsilon\right]\right\}\right)\right)\right|^2\right\}\\ &\overset{(a)}{=}\eta_k p_u\rho_k^2\left[n-\varepsilon\right]\sum_{l=1}^{L}\left|a_{kl}^*\left[n\right]\right|^2\mathbb{E}\left\{\left|\left(\hat{\mathbf{o}}_{kl}^{\mathrm{H}}\left[\varepsilon\right]\mathbf{o}_{kl}\left[\varepsilon\right]-\mathbb{E}\left\{\hat{\mathbf{o}}_{kl}^{\mathrm{H}}\left[\varepsilon\right]\mathbf{o}_{kl}\left[\varepsilon\right]\right\}\right)\right|^2\right\}\\ &=\eta_k p_u\rho_k^2\left[n-\varepsilon\right]\sum_{l=1}^{L}\left|a_{kl}^*\left[n\right]\right|^2\left(\mathbb{E}\left\{\left|\left(\hat{\mathbf{o}}_{kl}^{\mathrm{H}}\left[\varepsilon\right]\mathbf{o}_{kl}\left[\varepsilon\right]\right)\right|^2\right\}-\left|\mathbb{E}\left\{\hat{\mathbf{o}}_{kl}^{\mathrm{H}}\left[\varepsilon\right]\mathbf{o}_{kl}\left[\varepsilon\right]\right\}\right|^2\right)\\ &=\eta_k p_u\rho_k^2\left[n-\varepsilon\right]\sum_{l=1}^{L}\left|a_{kl}^*\left[n\right]\right|^2\mathrm{tr}\left(\boldsymbol{\Omega}_{kl}\mathbf{R}_{kl}\right). \end{aligned}\tag{41}$$

Then, we compute $\mathbb{E}\left\{\left|\hat{\mathbf{o}}_{kl}^{\mathrm{H}}\left[\varepsilon\right]\mathbf{o}_{il}\left[\varepsilon\right]\right|^2\right\}$. As for $i\in\mathcal{P}_k$, we can obtain

$$\begin{aligned}\mathbb{E}\left\{\left|\hat{\mathbf{o}}_{kl}^{\mathrm{H}}\left[\varepsilon\right]\mathbf{o}_{il}\left[\varepsilon\right]\right|^2\right\} &= \underbrace{\mathbb{E}\left\{\hat{\mathbf{o}}_{kl}^{\mathrm{H}}\left[\varepsilon\right]\hat{\mathbf{o}}_{il}\left[\varepsilon\right]\hat{\mathbf{o}}_{il}^{\mathrm{H}}\left[\varepsilon\right]\hat{\mathbf{o}}_{kl}\left[\varepsilon\right]\right\}}_{T_1}\\ &\quad+\underbrace{\mathbb{E}\left\{\hat{\mathbf{o}}_{kl}^{\mathrm{H}}\left[\varepsilon\right]\tilde{\mathbf{o}}_{il}\left[\varepsilon\right]\tilde{\mathbf{o}}_{il}^{\mathrm{H}}\left[\varepsilon\right]\hat{\mathbf{o}}_{kl}\left[\varepsilon\right]\right\}}_{T_2}. \end{aligned}\tag{37}$$

Using (10) and with the help of [33, Lemma B.14], we can obtain $T_1$ as

$$\begin{aligned}T_1 &= p_k p_i\rho_k^2\left[\varepsilon-t_k\right]\rho_i^2\left[\varepsilon-t_k\right]\left(\left|\mathrm{tr}\left(\boldsymbol{\Psi}_{kl}\mathbf{R}_{il}\mathbf{R}_{kl}\boldsymbol{\Psi}_{kl}\boldsymbol{\Psi}_{kl}^{-1}\right)\right|^2\right.\\ &\quad\left.+\mathrm{tr}\left(\boldsymbol{\Psi}_{kl}\mathbf{R}_{il}\mathbf{R}_{kl}\boldsymbol{\Psi}_{kl}\boldsymbol{\Psi}_{kl}^{-1}\left(\boldsymbol{\Psi}_{kl}\mathbf{R}_{il}\mathbf{R}_{kl}\boldsymbol{\Psi}_{kl}\right)^{\mathrm{H}}\boldsymbol{\Psi}_{kl}^{-1}\right)\right)\\ &=\left|\varpi_{ki,l}\right|^2+\mathrm{tr}\left(\boldsymbol{\Omega}_{kl}\boldsymbol{\Omega}_{il}\right). \end{aligned}\tag{38}$$

Consequently, we can derive $T_2$ as

$$\begin{aligned}T_2 &= \mathrm{tr}\left(\mathbb{E}\left\{\hat{\mathbf{o}}_{kl}\left[\varepsilon\right]\hat{\mathbf{o}}_{kl}^{\mathrm{H}}\left[\varepsilon\right]\right\}\mathbb{E}\left\{\tilde{\mathbf{o}}_{il}\left[\varepsilon\right]\tilde{\mathbf{o}}_{il}^{\mathrm{H}}\left[\varepsilon\right]\right\}\right)\\ &=\mathrm{tr}\left(\boldsymbol{\Omega}_{kl}\left(\mathbf{R}_{il}-\boldsymbol{\Omega}_{il}\right)\right). \end{aligned}\tag{39}$$

For the case of $i\notin\mathcal{P}_k$, we can obtain

$$\begin{aligned}&\mathbb{E}\left\{\left|\hat{\mathbf{o}}_{kl}^{\mathrm{H}}\left[\varepsilon\right]\mathbf{o}_{il}\left[\varepsilon\right]\right|^2\right\}=\mathrm{tr}\left(\mathbb{E}\left\{\hat{\mathbf{o}}_{kl}\left[\varepsilon\right]\hat{\mathbf{o}}_{kl}^{\mathrm{H}}\left[\varepsilon\right]\mathbf{o}_{il}\left[\varepsilon\right]\mathbf{o}_{il}^{\mathrm{H}}\left[\varepsilon\right]\right\}\right)\\ &=\rho_k^2\left[\varepsilon-t_k\right]p_k\mathrm{tr}\left(\mathbf{R}_{kl}\boldsymbol{\Psi}_{kl}\mathbf{R}_{kl}\mathbf{R}_{il}\right). \end{aligned}\tag{40}$$

By combining all above cases, we conclude that $\mathbb{E}\left\{\left|\hat{\mathbf{o}}_{kl}^{\mathrm{H}}\left[\lambda\right]\mathbf{o}_{il}\left[\lambda\right]\right|^2\right\}=\mathrm{tr}\left(\boldsymbol{\Omega}_{kl}\mathbf{R}_{il}\right)+\left|\varpi_{ki,l}\right|^2$, if $i\in\mathcal{P}_k$ and otherwise $\mathbb{E}\left\{\left|\hat{\mathbf{o}}_{kl}^{\mathrm{H}}\left[\lambda\right]\mathbf{o}_{il}\left[\lambda\right]\right|^2\right\}=\mathrm{tr}\left(\boldsymbol{\Omega}_{kl}\mathbf{R}_{il}\right)$.

Furthermore, based on the results in (36) and (40), we compute the beamforming uncertainty term as (41) at the top of this page, where (a) follows by the fact that the addends are independent random variables [4]. Note that the UE-RIS channel of the aggregate channels $\mathbf{o}_{kl}$ and $\mathbf{o}_{kl'}$ is independent because the signal transmitted by the same UE is reflected by different RISs. By applying [32, Eq. (28)], we can derive the channel aging term as

$$\begin{aligned}&\mathbb{E}\left\{\left|\mathrm{CA}_{k,n}\right|^2\right\}\\ &=\eta_k p_u\bar{\rho}_k^2\left[n-\varepsilon\right]\left(\sum_{l=1}^{L}\left|a_{kl}^*\left[n\right]\right|^2\mathbb{E}\left\{\left|\hat{\mathbf{o}}_{kl}^{\mathrm{H}}\left[\varepsilon\right]\mathbf{u}_{kl}\left[n\right]\right|^2\right\}\right.\\ &\left.+\sum_{l=1}^{L}\sum_{j=1,j\neq l}^{L}a_{kl}\left[n\right]a_{kj}^*\left[n\right]\mathbb{E}\left\{\left(\hat{\mathbf{o}}_{kl}^{\mathrm{H}}\left[\varepsilon\right]\mathbf{u}_{kl}\left[n\right]\right)\left(\hat{\mathbf{o}}_{kj}^{\mathrm{H}}\left[\varepsilon\right]\mathbf{u}_{kj}\left[n\right]\right)\right\}\right). \end{aligned}\tag{42}$$

As $\hat{\mathbf{o}}_{kl}\left[\varepsilon\right]$ and $\mathbf{u}_{kl}\left[n\right]$ are uncorrelated due to the definition of channel aging in (6), we obtain

$$\mathbb{E}\left\{\left|\hat{\mathbf{o}}_{kl}^{\mathrm{H}}\left[\varepsilon\right]\mathbf{u}_{kl}\left[n\right]\right|^2\right\}=\mathrm{tr}\left(\boldsymbol{\Omega}_{kl}\mathbf{R}_{kl}\right).\tag{43}$$

$$\sum_{l=1}^{L}\sum_{j=1,j\neq l}^{L}a_{kl}\left[n\right]a_{kj}^*\left[n\right]\mathbb{E}\left\{\left(\hat{\mathbf{o}}_{kl}^{\mathrm{H}}\left[\varepsilon\right]\mathbf{u}_{kl}\left[n\right]\right)\left(\hat{\mathbf{o}}_{kj}^{\mathrm{H}}\left[\varepsilon\right]\mathbf{u}_{kj}\left[n\right]\right)\right\}=0.\tag{44}$$

Then, putting (42)-(44) together yields

$$\mathbb{E}\left\{\left|\mathrm{CA}_{k,n}\right|^2\right\}=\eta_k p_u\bar{\rho}_k^2\left[n-\varepsilon\right]\sum_{l=1}^{L}\left|a_{kl}^*\left[n\right]\right|^2\mathrm{tr}\left(\boldsymbol{\Omega}_{kl}\mathbf{R}_{kl}\right).\tag{45}$$

Subsequently, by applying [32, Eq. (29)], we compute $\mathbb{E}\left\{\left|\mathrm{UI}_{k,n}\right|^2\right\}$ as

$$\begin{aligned}&\mathbb{E}\left\{\left|\mathrm{UI}_{k,n}\right|^2\right\}=\eta_i p_u\mathbb{E}\left\{\left|\sum_{l=1}^{L}a_{kl}^*\left[n\right]\hat{\mathbf{o}}_{kl}^{\mathrm{H}}\left[\varepsilon\right]\mathbf{o}_{il}\left[\varepsilon\right]\right|^2\right\}\\ &=\eta_i p_u\sum_{l=1}^{L}\left|a_{kl}^*\left[n\right]\right|^2\underbrace{\mathbb{E}\left\{\left|\hat{\mathbf{o}}_{kl}^{\mathrm{H}}\left[\varepsilon\right]\mathbf{o}_{il}\left[n\right]\right|^2\right\}}_{T_3}\\ &+\eta_i p_u\sum_{l=1}^{L}\sum_{j=1,j\neq l}^{L}a_{kl}\left[n\right]a_{kj}^*\left[n\right]\underbrace{\mathbb{E}\left\{\left(\hat{\mathbf{o}}_{kl}^{\mathrm{H}}\left[\varepsilon\right]\mathbf{o}_{il}\left[n\right]\right)^*\left(\hat{\mathbf{o}}_{kj}^{\mathrm{H}}\left[\varepsilon\right]\mathbf{o}_{ij}\left[n\right]\right)\right\}}_{T_4}. \end{aligned}\tag{46}$$

By utilizing (14), we have

$$\begin{aligned}T_3 &= \rho_i^2 [n-\varepsilon] \mathbb{E}\left\{\left|\hat{\mathbf{o}}_{kl}^{\mathrm{H}}[\varepsilon]\mathbf{o}_{il}[\varepsilon]\right|^2\right\} \\ &+ \bar{\rho}_i^2 [n-\varepsilon] \mathbb{E}\left\{\left|\hat{\mathbf{o}}_{kl}^{\mathrm{H}}[\varepsilon]\mathbf{u}_{il}[n]\right|^2\right\} \\ &= \rho_i^2 [n-\varepsilon] \mathrm{tr}\left(\mathbf{\Omega}_{kl}\mathbf{R}_{il}\right) + \bar{\rho}_i^2 [n-\varepsilon] \mathrm{tr}\left(\mathbf{\Omega}_{kl}\mathbf{R}_{il}\right) \\ &+ \begin{cases} \rho_i^2 [n-\varepsilon] |\varpi_{ki,l}|^2, & i \in \mathcal{P}_k \\ 0, & i \notin \mathcal{P}_k. \end{cases} \\ &= \mathrm{tr}\left(\mathbf{\Omega}_{kl}\mathbf{R}_{il}\right) + \begin{cases} \rho_i^2 [n-\varepsilon] |\varpi_{ki,l}|^2, & i \in \mathcal{P}_k \\ 0, & i \notin \mathcal{P}_k. \end{cases} \end{aligned} \tag{47}$$

$$\begin{aligned}T_4 &= \rho_i^2 [n-\varepsilon] \mathbb{E}\left\{\hat{\mathbf{o}}_{kl}^{\mathrm{H}}[\varepsilon]\mathbf{o}_{il}[\varepsilon]\right\} \mathbb{E}\left\{\hat{\mathbf{o}}_{kj}^{\mathrm{H}}[\varepsilon]\mathbf{o}_{ij}[\varepsilon]\right\} \\ &= \begin{cases} \rho_i^2 [n-\varepsilon] \varpi_{ki,l}\varpi_{ki,j}, & i \in \mathcal{P}_k \\ 0, & i \notin \mathcal{P}_k. \end{cases} \end{aligned} \tag{48}$$

After substituting $T_3$ and $T_4$ into (46), we can obtain

$$\begin{aligned}\mathbb{E}\left\{|\mathrm{UI}_{k,n}|^2\right\} &= \eta_i p_u \sum_{l=1}^{L} |a_{kl}^*[n]|^2 \mathrm{tr}\left(\mathbf{\Omega}_{kl}\mathbf{R}_{il}\right) \\ &+ \begin{cases} \eta_i p_u \rho_i^2 [n-\varepsilon] \left|\sum_{l=1}^{L} a_{kl}^*[n]\varpi_{ki,l}\right|^2, & i \in \mathcal{P}_k \\ 0, & i \notin \mathcal{P}_k. \end{cases} \end{aligned} \tag{49}$$

We compute $\mathbb{E}\left\{|\mathrm{NS}_{k,n}|^2\right\}$ which is similar to the term in the numerator as

$$\begin{aligned}\mathbb{E}\left\{|\mathrm{NS}_{k,n}|^2\right\} &= \sigma_u^2 \mathbb{E}\left\{\left|\sum_{l=1}^{L} a_{kl}^*[n]\hat{\mathbf{o}}_{kl}^{\mathrm{H}}[\varepsilon]\right|^2\right\} \\ &= \sigma_u^2 \sum_{l=1}^{L} |a_{kl}^*[n]|^2 \mathrm{tr}\left(\mathbf{\Omega}_{kl}\right). \end{aligned} \tag{50}$$

Finally, substituting the above results into (18) and the results for the uplink SE follow.

## REFERENCES


[1] M. Giordani, M. Polese, M. Mezzavilla, S. Rangan, and M. Zorzi, "Toward 6G networks: Use cases and technologies," *IEEE Commun. Mag.*, vol. 58, no. 3, pp. 55–61, Mar. 2020.

[2] H. Q. Ngo, A. Ashikhmin, H. Yang, E. G. Larsson, and T. L. Marzetta, "Cell-free massive MIMO versus small cells," *IEEE Trans. Wireless Commun.*, vol. 16, no. 3, pp. 1834–1850, Mar. 2017.

[3] E. Björnson and L. Sanguinetti, "Making cell-free massive MIMO competitive with MMSE processing and centralized implementation," *IEEE Trans. Wireless Commun.*, vol. 19, no. 1, pp. 77–90, Jan. 2019.

[4] Ö. Özdogan, E. Björnson, and J. Zhang, "Performance of cell-free massive MIMO with Rician fading and phase shifts," *IEEE Trans. Wireless Commun.*, vol. 18, no. 11, pp. 5299–5315, Nov. 2019.

[5] Z. Wang, J. Zhang, B. Ai, C. Yuen, and M. Debbah, "Uplink performance of cell-free massive MIMO with multi-antenna users over jointly-correlated Rayleigh fading channels," *IEEE Trans. Wireless Commun.*, vol. 21, no. 9, pp. 7391–7406, Sep. 2022.

[6] T. Van Chien, H. Q. Ngo, S. Chatzinotas, M. Di Renzo, and B. Ottersten, "Reconfigurable intelligent surface-assisted cell-free massive MIMO systems over spatially-correlated channels," *IEEE Trans. Wireless Commun.*, vol. 21, no. 7, pp. 5106–5128, Jul. 2022.

[7] Q. Wu and R. Zhang, "Towards smart and reconfigurable environment: Intelligent reflecting surface aided wireless network," *IEEE Commun. Mag.*, vol. 58, no. 1, pp. 106–112, Jan. 2019.

[8] C. Huang, A. Zappone, G. C. Alexandropoulos, M. Debbah, and C. Yuen, "Reconfigurable intelligent surfaces for energy efficiency in wireless communication," *IEEE Trans. Wireless Commun.*, vol. 18, no. 8, pp. 4157–4170, Aug. 2019.

[9] L. Yang, Y. Yang, M. O. Hasna, and M.-S. Alouini, "Coverage, probability of SNR gain, and DOR analysis of RIS-aided communication systems," *IEEE Wireless Commun. Lett.*, vol. 9, no. 8, pp. 1268–1272, Aug. 2020.

[10] E. Björnson and L. Sanguinetti, "Rayleigh fading modeling and channel hardening for reconfigurable intelligent surfaces," *IEEE Wireless Commun. Lett.*, vol. 10, no. 4, pp. 830–834, Apr. 2020.

[11] E. Shi, J. Zhang, R. He, H. Jiao, Z. Wang, B. Ai, and D. W. K. Ng, "Spatially correlated reconfigurable intelligent surfaces-aided cell-free massive MIMO systems," *IEEE Trans. Veh. Technol.*, vol. 71, no. 8, pp. 775–779, Aug. 2022.

[12] S. Dhok and P. K. Sharma, "Rate-splitting multiple access with STAR RIS over spatially-correlated channels," *IEEE Trans. Commun.*, vol. 70, no. 10, pp. 6410–6424, Oct. 2022.

[13] Z. Zhang and L. Dai, "A joint precoding framework for wideband reconfigurable intelligent surface-aided cell-free network," *IEEE Trans. on Signal Process.*, vol. 69, no. 6, pp. 4085–4101, Jun. 2021.

[14] E. Shi, J. Zhang, S. Chen, J. Zheng, Y. Zhang, D. W. Kwan Ng, and B. Ai, "Wireless energy transfer in RIS-aided cell-free massive MIMO systems: Opportunities and challenges," *IEEE Commun. Mag.*, vol. 60, no. 3, pp. 26–32, Mar. 2022.

[15] X. Ma, D. Zhang, M. Xiao, C. Huang, and Z. Chen, "Cooperative beamforming for RIS-aided cell-free massive MIMO networks," *IEEE Trans. Wireless Commun.*, vol. 22, no. 11, pp. 7243–7258, Nov. 2023.

[16] X. Gan, C. Zhong, C. Huang, Z. Yang, and Z. Zhang, "Multiple RISs assisted cell-free networks with two-timescale CSI: Performance analysis and system design," *IEEE Trans. Commun.*, vol. 70, no. 11, pp. 7696–7710, Nov. 2022.

[17] N. T. Nguyen, V.-D. Nguyen, H. Van Nguyen, H. Q. Ngo, S. Chatzinotas, and M. Juntti, "Spectral efficiency analysis of hybrid relay-reflecting intelligent surface-assisted cell-free massive MIMO systems," *IEEE Trans. Wireless Commun.*, vol. 22, no. 5, pp. 3397–3416, May 2023.

[18] C. Chen, S. Xu, J. Zhang, and J. Zhang, "A distributed machine learning-based approach for IRS-enhanced cell-free MIMO networks," *IEEE Trans. Wireless Commun., early access*, 2023.

[19] S. Buzzi, C. D'Andrea, A. Zappone, M. Fresia, Y.-P. Zhang, and S. Feng, "RIS configuration, beamformer design, and power control in single-cell and multi-cell wireless networks," *IEEE Trans. Cognit. Commun. Networking*, vol. 7, no. 2, pp. 398–411, Feb. 2021.

[20] M. Alonzo, S. Buzzi, A. Zappone, and C. D'Elia, "Energy-efficient power control in cell-free and user-centric massive MIMO at millimeter wave," *IEEE Trans. Green Commun. Networking*, vol. 3, no. 3, pp. 651–663, Mar. 2019.

[21] K. T. Truong and R. W. Heath, "Effects of channel aging in massive MIMO systems," *J. Commun. Netw.*, vol. 15, no. 4, pp. 338–351, Apr. 2013.

[22] J. Yuan, H. Q. Ngo, and M. Matthaiou, "Machine learning-based channel prediction in massive MIMO with channel aging," *IEEE Trans. Wireless Commun.*, vol. 19, no. 5, pp. 2960–2973, May 2020.

[23] A. K. Papazafeiropoulos, "Impact of general channel aging conditions on the downlink performance of massive MIMO," *IEEE Trans. Veh. Technol.*, vol. 66, no. 2, pp. 1428–1442, Feb. 2017.

[24] A. Papazafeiropoulos, I. Krikidis, and P. Kourtessis, "Impact of channel aging on reconfigurable intelligent surface aided massive MIMO systems with statistical CSI," *IEEE Trans. Veh. Technol.*, vol. 72, no. 1, pp. 689–703, Jan. 2022.

[25] Y. Zhang, J. Zhang, H. Xiao, D. W. K. Ng, and B. Ai, "Channel aging-aware precoding for RIS-aided multi-user communications," *IEEE Trans. Veh. Technol., early access*, vol. 72, no. 2, pp. 1997–2008, Feb. 2023.

[26] R. Chopra, C. R. Murthy, and A. K. Papazafeiropoulos, "Uplink performance analysis of cell-free mMIMO systems under channel aging," *IEEE Commun. Lett.*, vol. 25, no. 7, pp. 2206–2210, Jul. 2021.

[27] J. Zheng, J. Zhang, E. Björnson, and B. Ai, "Impact of channel aging on cell-free massive MIMO over spatially correlated channels," *IEEE Trans. Wireless Commun.*, vol. 20, no. 10, pp. 6451–6466, Oct. 2021.

[28] B. Li, L.-L. Yang, R. G. Maunder, S. Sun, and P. Xiao, "Multicarrier-division duplex for solving the channel aging problem in massive MIMO systems," *IEEE Transactions on Vehicular Technology*, vol. 72, no. 2, pp. 1940–1954, Feb. 2022.

[29] M. Abramowitz and I. A. Stegun, *Handbook of mathematical functions with formulas, graphs, and mathematical tables*. US Government printing office, 1964, vol. 55.

[30] E. Björnson, M. Matthaiou, and M. Debbah, "Massive MIMO with non-ideal arbitrary arrays: Hardware scaling laws and circuit-aware design," *IEEE Trans. Wireless Commun.*, vol. 14, no. 8, pp. 4353–4368, Aug. 2015.

[31] A. Papazafeiropoulos, C. Pan, P. Kourtessis, S. Chatzinotas, and J. M. Senior, "Intelligent reflecting surface-assisted MU-MISO systems with imperfect hardware: Channel estimation and beamforming design," *IEEE Trans. Wireless Commun.*, vol. 21, no. 3, pp. 2077–2092, Mar. 2021.
[32] J. Zheng, J. Zhang, L. Zhang, X. Zhang, and B. Ai, "Efficient receiver design for uplink cell-free massive MIMO with hardware impairments," *IEEE Trans. Veh. Technol.*, vol. 69, no. 4, pp. 4537–4541, Apr. 2020.
[33] E. Björnson, J. Hoydis, L. Sanguinetti *et al.*, "Massive MIMO networks: Spectral, energy, and hardware efficiency," *Foundations and Trends® in Signal Processing*, vol. 11, no. 3-4, pp. 154–655, 2017.
[34] Z. Chen and E. Björnson, "Channel hardening and favorable propagation in cell-free massive MIMO with stochastic geometry," *IEEE Trans. Commun.*, vol. 66, no. 11, pp. 5205–5219, Nov. 2018.

**Enyu Shi** received the B.S. degree in communication engineering from Beijing Jiaotong University, China, in 2019, where he is currently pursuing the Ph.D. degree. He is also a Visiting Scholar with the School of Electrical and Electronic Engineering, Nanyang Technological University (NTU), Singapore. His research interests include cell-free massive multiple-input multiple-output (MIMO) systems, reconfigurable intelligent surface (RIS), signal processing, and performance analysis of wireless systems. He serves as a Reviewer for IEEE TRANSACTIONS ON WIRELESS COMMUNICATIONS, and IEEE TRANSACTIONS ON COMMUNICATIONS.

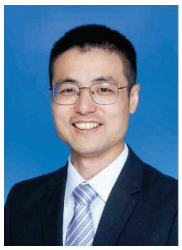

**Jiayi Zhang** (S'08-M'14-SM'20) received the B.Sc. and Ph.D. degree of Communication Engineering from Beijing Jiaotong University, China in 2007 and 2014, respectively. Since 2016, he has been a Professor with School of Electronic and Information Engineering, Beijing Jiaotong University, China. From 2014 to 2016, he was a Postdoctoral Research Associate with the Department of Electronic Engineering, Tsinghua University, China. From 2014 to 2015, he was also a Humboldt Research Fellow in Institute for Digital Communications, Friedrich-Alexander-University Erlangen-Nürnberg (FAU), Germany. From 2012 to 2013, he was a visiting scholar at the Wireless Group, University of Southampton, United Kingdom. His current research interests include cell-free massive MIMO, reconfigurable intelligent surface (RIS), XL-MIMO, near-field communications and applied mathematics.

Dr. Zhang received the Best Paper Awards at the IEEE ICC 2023, the URSI Young Scientist Award in 2020, and the IEEE ComSoc Asia-Pacific Outstanding Young Researcher Award in 2020. He was the Lead Guest Editor of the special issue on "Multiple Antenna Technologies for Beyond 5G" of the IEEE JOURNAL ON SELECTED AREAS IN COMMUNICATIONS, the Lead Guest Editor of the special issue on "Semantic Communications for the Metaverse" of the IEEE WIRELESS COMMUNICATIONS and an Editor for IEEE COMMUNICATIONS LETTERS from 2016-2021. He currently serves as an Associate Editor for IEEE TRANSACTIONS ON COMMUNICATIONS and IEEE TRANSACTIONS ON WIRELESS COMMUNICATIONS.

**Jiakang Zheng** (jiakangzheng@bjtu.edu.cn) received the B.S. degree in the School of Electronic and Information Engineering from Beijing Jiaotong University (BJTU), China, in 2019, where he is currently pursuing the Ph.D. degree. He is also a Visiting Scholar with the School of Computer Science and Engineering, Nanyang Technological University (NTU), Singapore. His research interests include cell-free massive MIMO systems, resource allocation and performance analysis of wireless systems. He serves as a Reviewer for IEEE JOURNAL ON SELECTED AREAS IN COMMUNICATIONS, IEEE TRANSACTIONS ON WIRELESS COMMUNICATIONS, and IEEE TRANSACTIONS ON COMMUNICATIONS.

**Derrick Wing Kwan Ng (S'06-M'12-SM'17-F'21)** received his bachelor's degree (with first-class Honors) and the Master of Philosophy degree in electronic engineering from The Hong Kong University of Science and Technology (HKUST), Hong Kong, in 2006 and 2008, respectively, and his Ph.D. degree from The University of British Columbia, Vancouver, BC, Canada, in November 2012. He was a senior postdoctoral fellow at the Institute for Digital Communications, Friedrich-Alexander-University Erlangen-Nürnberg (FAU), Germany. He is currently a Scientia Associate Professor with the University of New South Wales, Sydney, NSW, Australia. His research interests include global optimization, physical layer security, IRS-assisted communication, UAV-assisted communication, wireless information and power transfer, and green (energy-efficient) wireless communications.

Since 2018, he has been listed as a Highly Cited Researcher by Clarivate Analytics (Web of Science). He was the recipient of the Australian Research Council (ARC) Discovery Early Career Researcher Award 2017, IEEE Communications Society Leonard G. Abraham Prize 2023, IEEE Communications Society Stephen O. Rice Prize 2022, Best Paper Awards at the WCSP 2020, 2021, IEEE TCGCC Best Journal Paper Award 2018, INISCOM 2018, IEEE International Conference on Communications (ICC) 2018, 2021, 2023, IEEE International Conference on Computing, Networking and Communications (ICNC) 2016, IEEE Wireless Communications and Networking Conference (WCNC) 2012, IEEE Global Telecommunication Conference (Globecom) 2011, 2021, and IEEE Third International Conference on Communications and Networking in China 2008. From January 2012 to December 2019, he served as an Editorial Assistant to the Editor-in-Chief of the IEEE Transactions on Communications. He is also the Editor of the IEEE Transactions on Communications and an Associate Editor-in-Chief for the IEEE Open Journal of the Communications Society.

**Bo Ai** (Fellow, IEEE) received his Master degree and Ph. D. degree from Xidian University in China. He graduated from Tsinghua University with the honor of Excellent Postdoctoral Research Fellow at Tsinghua University in 2007. He was a visiting professor at EE Department, Stanford University in 2015. He is now working at Beijing Jiaotong University as a full professor and Ph. D. candidate advisor. He is the Deputy Director of State Key Lab of Rail Traffic Control and Safety, and the Deputy Director of International Joint Research Center. He is one of the main responsible people for Beijing "Urban rail operation control system" International Science and Technology Cooperation Base, and the backbone member of the Innovative Engineering Based jointly granted by Chinese Ministry of Education and the State Administration of Foreign Experts Affairs.

He has authored/co-authored 8 books and published over 300 academic research papers in his research area. He has hold 26 invention patents. He has been the research team leader for 26 national projects and has won some important scientific research prizes. Five papers have been the ESI highly-cited paper. He has been notified by Council of Canadian Academies (CCA) that, based on Scopus database, Prof. Bo Ai has been listed as one of the Top 1% authors in his field all over the world. Prof. Bo Ai has also been Feature Interviewed by IET ELECTRONICS LETTERS. His interests include the research and applications of channel measurement and channel modeling, dedicated mobile communications for rail traffic systems.

Prof. Bo Ai is a Fellow of the Institution of Engineering and Technology (IET Fellow), IEEE VTS Distinguished Lecturer. He is an IEEE VTS Beijing Chapter Vice Chair. IEEE BTS Xi'an Chapter Chair. He was as a Co-chair or a Session/Track Chair for many international conferences. He is an associate editor of IEEE ANTENNAS AND WIRELESS PROPAGATION LETTERS, IEEE TRANSACTIONS ON CONSUMER ELECTRONICS and an Editorial Committee Member of the Wireless Personal Communications journal. He is the Lead Guest Editor for Special Issues on IEEE TRANSACTIONS ON VEHICULAR TECHNOLOGY, IEEE ANTENNAS AND PROPAGATIONS LETTERS, INTERNATIONAL JOURNAL ON ANTENNAS AND PROPAGATIONS. He has received many awards such as Distinguished Youth Foundation and Excellent Youth Foundation from National Natural Science Foundation of China, the Qiushi Outstanding Youth Award by Hong Kong Qiushi Foundation, the New Century Talents by the Chinese Ministry of Education, the Zhan Tianyou Railway Science and Technology Award by the Chinese Ministry of Railways, and the Science and Technology New Star by the Beijing Municipal Science and Technology Commission.